C.P. No. 585

C.P. No. 585

MINISTRY OF AVIATION

AERONAUTICAL RESEARCH COUNCIL

CURRENT PAPERS

An Experimental Investigation of the Characteristics of an Ogee Wing from M=0·4 to M=1·8

by

L. C. Squire

and

D. S. Capps

LONDON: HER MAJESTY'S STATIONERY OFFICE

1962

PRICE 5s 6d NET

U.D.C. No.533.693.3:533.6.011.34/5:533.6.013.412

C.P. No. 585

August, 1959

AN EXPERIMENTAL INVESTIGATION OF THE CHARACTERISTICS OF AN OGEE WING FROM M = 0.4 to M = 1.8

by

L.C. Squire

and

D.S. Capps

SUMMARY

Wind tunnel tests have been made in the 3 ft tunnel at R.A.E. Bedford to investigate the flow development and longitudinal static stability of a slender ogee wing (aspect ratio 1.2) from M = 0.4 to M = 1.82. Throughout the Mach number range the flow separates from the leading edge at some positive incidence and a pair of vortices lie above the wing. This leading edge separation occurs at very low incidence at subsonic speeds but at supersonic speeds occurs at progressively higher incidences as the Mach number increases. The additional lift associated with the vortices is approximately independent of Mach number at subsonic speeds but at supersonic speeds the additional lift decreases with increase in Mach number. The overall rearward shift in aerodynamic centre position and centre of pressure position between subsonic and supersonic speeds is 6% of the root chord

---

Previously issued as R.A.E. Tech Note No. Aero.2648 - A.R.C.21,798

LIST OF CONTENTS

TABLE

LIST OF ILLUSTRATIONS

LIST OF ILLUSTRATIONS (Contd.)

1 INTRODUCTION

In connection with the design of slender wings for supersonic flight various considerations have led to studies of slender planforms with curved leading edges. However, these studies have been hampered by a lack of information on the movement of aerodynamic centre on these planforms throughout the Mach number range, in particular at transonic speeds. This Note gives results of wind tunnel tests on an ogee planform* from M = 0.4 to M = 1.8. In addition to data on the aerodynamic centre movement the tests also provide information on the variation of drag due to lift with Mach number.

2 EXPERIMENTAL DETAILS

2.1 Details of the model

Details of the model are given in Fig.1; basically it consisted of a slender wing of aspect ratio 1.2 mounted on a simple circular body. The wing sections normal to the stream were rhombic and the root section was of parabolic biconvex shape with a thickness chord ratio of 5%. The circular body was the full length of the wing (20 inches); over the rear half of the wing the body had a constant diameter of 1.6 inches. The front of the body was ogival in form.

The rear, parallel part of the model was made of steel and was bolted to a metal plate inside the wing, this metal plate was used to attach the model to the sting support. The rest of the model was made of glass-cloth and araldite cast onto the body and the internal metal plate.

2.2 Details of the tests

Tests were made in the speed range from M = 0.4 to 1.82 in the transonic and supersonic working sections of the R.A.E., Bedford, 3 ft tunnel. All tests were made at zero sideslip.

Lift, pitching moment and drag were measured at Mach numbers of 0.4, 0.7, 0.8, 0.85, 0.9, 0.94, 0.98, 1.00, 1.02, 1.04, 1.06, 1.08, 1.10, 1.15, 1.20 and 1.25 through an incidence range from -2° to $+13^{\circ}$ in the transonic working section, and at Mach numbers of 1.32, 1.42, 1.61 and 1.82 through an incidence range from -2° to $+10^{\circ}$ in the supersonic working section. In addition to these force tests a series of oil flow patterns were obtained at Mach numbers of 0.7 and 1.61 and a series of vapour screen photographs at M = 1.61.

The force tests were made with transition fixed by means of a band of distributed roughness 0.5 inch wide the whole length of the leading edge; this band began 0.125 inch back from the edge to ensure that the edge remained sharp. At subsonic and transonic speeds the roughness consisted of carborundum particles 0.003 inch high, whereas at supersonic speeds the particles were 0.007 inch high. Transition was not fixed in the flow visualisation tests since the main interest was in the flow near the leading edge and the presence of roughness would have obscured the flow pattern in this region. Both force and flow visualisation tests were made at a Reynolds number of 1.7×10^{6} based on aerodynamic mean chord.

The results of the force tests between M = 1.02 and 1.20 are liable to wind tunnel interference due to the reflection of the model flow field by the tunnel walls; these results are not presented in this Note, but they have

---

*The term 'ogee' has been used to describe slender wings which have a point of inflection in their leading edge shape (see Fig.1)

been used to draw faired curves between results outside the region of interference.

Below M = 1.0 the results may be liable to some wind tunnel interference, however, this is probably small at low incidence but may increase at the higher incidences. No detailed data is available on the actual magnitude of this interference on slender configurations but results on other models[1] suggest that at the maximum incidence the true lift coefficients may be about 2% higher than the quoted values. In addition, near M = 1.0 the quoted Mach number may be about 0.005 higher than the true Mach number.

Apart from this wind tunnel interference it is estimated that 95% of the results have accuracies within the following limits:-

C_L = ±0.003

C_m = ±0.0005

C_D = ±0.0004 at $C_L = 0$

±0.001 at $C_L = 0.3$

α = ±0.05

The drag results have been corrected to a base pressure equal to free stream static pressure and the pitching moments are referred to the mean quarter chord point.

The force results, except those in the Mach number range from M = 1.02 to 1.20, are tabulated in Table 1.

3 DISCUSSION OF RESULTS

3.1 Lift and pitching moment

The variation of C_L with α, and of C_m with C_L, is presented in Figs.2 to 5. The variation of C_L with Mach number at fixed incidence is given in Fig.6 and the movements of aerodynamic centre and centre of pressure position with Mach number in Figs.7 and 8. The outstanding feature of the lift and pitching moment curves (Figs.2-5) is the marked non-linearity of the lift curves (particularly at subsonic speeds) compared with the almost linear character of the pitching moment curves.

Considering the lift curves in more detail, it will be seen that at subsonic speeds the non-linear increase in lift associated with leading edge separation and rolled up vortex sheets is apparent from very low incidence. This increase in lift is illustrated at M = 1.0 by comparing the experimental lift with slender wing theory $C_L = \frac{\pi A}{2} \alpha$ (radians), (Fig.2). At low incidence the lift is just above the slender wing value but at 10° the measured lift coefficient is 0.454 compared with the slender value of 0.330.

For slender delta wings Mangler and Smith[2] have shown that the additional lift due to the vortices is approximately $4\alpha^2$ (α in radians). Various other simpler theories[3,4,5,6,7] lead to non-linear lift of the form $k\alpha^{5/3}$, where the coefficient k varies from 3.3 to 7.2 in the different theories for the present wing*.

---

* Actually for the delta wing of the same aspect ratio.

When $4\alpha^2$ was added to the slender wing lift fairly good agreement with the measured lift was obtained at M = 1.0 (see Fig.6). Below M = 1.0 the lift at a given incidence decreases with decrease in Mach number: the decrease is similar to that given by linear theory for a delta wing of the same aspect ratio i.e. the delta formed by joining the apex to the wing tips. This lift is plotted in Fig.6 when it is labelled $\left(\frac{\partial \bar{C}_L}{\partial \alpha}\right)_\Delta \alpha$. Also plotted in Fig.6 is the linear lift plus $4\alpha^2$. In general this theoretical lift is in fair agreement with experiment, although the experimental lift is lower than the theoretical values at M = 0.4. Much better agreement with experiment is obtained if the $\alpha^{5/3}$ form of non-linear lift is used with a coefficient of 2. This non-linear lift has also been added to the linear lift and plotted in Fig.6, and the agreement is now very good throughout the incidence range at Mach numbers below 1.0. At M = 0.4, for example, the measured lift is about 1% below $\left(\frac{\partial \bar{C}_L}{\partial \alpha}\right)_\Delta \alpha + 2\alpha^{5/3}$ for all incidences, and at M = 0.7 the measured lift is in exact agreement. Above M = 0.7 the measured lift is slightly higher than $\left(\frac{\partial \bar{C}_L}{\partial \alpha}\right)_\Delta \alpha + 2\alpha^{5/3}$ throughout the incidence range except at M = 0.98 and 1.00 where the measured lift falls off at the higher incidences, possibly due to the interaction of shock waves with the vortices.

These results show that on this wing the non-linear lift associated with the leading edge separations is almost independent of Mach number below M = 1.0. An analysis of results between M = 1.0 and M = 1.2 showed that the non-linear lift remained of the same form and magnitude throughout this speed range, but began to decrease thereafter.

In Figs.9-11 oil flow patterns at M = 0.7 and M = 1.61 are compared at approximately the same incidence. The oil flow patterns at M = 0.70 confirm that there are large leading edge separations on this wing at subsonic speeds even at low incidence. For example at 2° incidence at M = 0.7 (Fig.9) the oil patterns show the typical streamline pattern of a leading edge separation with a rolled up vortex sheet. The attachment line, that is the dividing line between the streamwise flow inboard and the outward spanwise flow near the leading edge, follows the leading edge shape and is at approximately 90% of the local span along the whole leading edge. Outboard of the attachment line the oil streamlines run together into a thick oil line just inboard of the leading edge; this running together of the streamlines indicates that a secondary separation is taking place under the rolled up vortex sheet[8]. At 4° incidence (Fig.10) both the attachment and secondary separation lines have moved inboard and their shapes tend to follow the curve of the leading edge. The oil lines outboard of the secondary separation line are consistent with a second vortex lying along the leading edge under the main vortex sheet and rotating in the opposite direction. In general the flow pattern at 8° incidence (Fig.11) is similar to that at 4°; the attachment and separation lines are further inboard but still follow the shape of the leading edge. Outboard of the separation the flow pattern almost certainly indicates a secondary vortex, in particular close to the leading edge, at about 1/3 of the chord from the nose, the oil lines near the leading edge flow towards the edge, whereas just a little further inboard the flow direction is more streamwise. This pattern would tend to indicate a second attachment line with the flow inboard of this line flowing into the separated region of the main vortex.

Turning now to the lift at supersonic speeds there are two main differences from subsonic speeds, first there appears to be a region of linear lift curve near zero incidence, the extent of this region of linear

lift increasing with Mach number, and secondly when the non-linear lift is apparent it is less than at subsonic speeds. These trends are shown in both Figs.3 and 6. At M = 1.8 for example the lift curve appears linear up to 4° incidence and at 10° incidence the increment in non-linear lift is only 0.020 in C_L. At M = 1.0 the non-linear lift increment at 10° is 0.124. It should be noted that at M = 1.82 the slope of the linear lift is about 15% higher than that of the corresponding delta and in fact agrees with the slope given by slender body theory. The region of linear lift near zero incidence can be explained by the results analysed in Reference 9. Here it was shown that on a swept edge at supersonic speeds the flow did not separate from the edge until some positive incidence when the Mach number normal to edge was greater than about 0.6. In fact 4° at M = 1.8 lies just above the boundary for attached flow if the wing leading edge sweep is taken as that of the delta of the same aspect ratio. The absence of leading edge separations at low incidence is confirmed by the oil flow photographs at M = 1.61 of Figs.9-11. At 2° incidence, Fig.9, the oil flow pattern does not have the characteristic pattern of a leading edge vortex (see M = 0.7 in the same figure); instead the oil shows a number of streamwise streaks, between which the oil flows almost parallel to the leading edge. Similar patterns have been found and investigated in the flow over some 65° delta wings[10] where it was found that these streamwise streaks are associated with small vortices, probably within the boundary layer, which lie along the wing in the stream direction. These vortices did not appear to produce any non-linear lift. At 4° incidence there is an attachment line along the leading edge, in about the same position at both Mach numbers. Over the front part of the wing the oil patterns at these two Mach numbers are very similar. Over the rear portion of the wing marked differences occur. At M = 0.7 the oil outboard of the vortex is very well defined with clear streamlines under the vortex and a large amount of oil at the separation line, at M = 1.6 on the other hand the oil has not really moved outboard of the attachment line. This lack of oil movement is due to a shortage of running time; in fact at 8° incidence a similar pattern was first obtained and the pattern shown in Fig.11 required at least 3 times the usual running time to fully develop. This increase in running time is much greater than could be attributed to changes in oil mixture or model temperature, thus it would appear that at M = 1.6 the vortex is either weaker, or further from the surface, than at M = 0.7. However, photographs of the vapour screen 1 inch ahead of the trailing edge (Fig.12) show that the separated sheet is close to the wing surface. Thus, taken in conjunction with the loss of non-linear lift between M = 0.7 and 1.6, it would appear that there is a weaker vortex under the separation at M = 1.6 than at M = 0.7.

At 8° incidence the oil flow patterns at M = 0.7 and 1.6 both reveal a large vortex above the wing inboard of the leading edge, however, there are significant differences in the two flow patterns. At M = 1.6 the attachment line is further inboard and appears straighter than at 0.7, and the area of cross flow between the attachment line and the secondary separation is greater at the higher Mach number. The secondary separation at 1.6 is also slightly further from the leading edge than at M = 0.7. Under the vortex the oil streamlines at M = 1.61 do not have such a marked inflection point as at M = 0.70; however, without detailed calculations of flow directions the oil flow pattern does not reveal any obvious reasons for the lower non-linear lift at M = 1.61.

Turning now to the moment results it will be seen that in general the curves are much more linear than the lift curves. At M = 0.4 there is a very slight decrease in stability with increase in C_L, this decrease is, however, quite small and corresponds to a forward shift of about $\frac{1}{2}$% of root chord in the centre of pressure position between C_L = 0.1 and 0.5, the change in aerodynamic centre position is about 1.5% c_o between the same values of C_L. At M = 0.7 and 0.8 the aerodynamic centre is constant (within the accuracy of the results) throughout the lift range up to C_L = 0.6. At M = 0.85 and 0.90

the aerodynamic centre is again constant up to $C_L = 0.3$ but above this C_L there is a steady increase in stability, for example at M = 0.9 the aerodynamic centre moves back by 2% c_o with increase of C_L from $C_L = 0.3$ to $C_L = 0.5$. At M = 0.94 and 0.98 there is a region of reduced stability near zero incidence, at M = 0.94 for example, the aerodynamic centre at $C_L = 0$ is at about* 64% of the root chord compared with 66.7% at $C_L = 0.1$. Above $C_L = 0.1$ the stability again increases at M = 0.94, as at 0.90. Above M = 1.0, up to M = 1.8, the pitching moment curves vary linearly with lift and there are no significant changes in aerodynamic centre or centre of pressure position.

The total movements of aerodynamic centre and centre of pressure, at various C_L's, with Mach number are summarised in the curves of Figs.7 and 8. In Fig.7 is also plotted the linear theory (attached flow) aerodynamic centre position for a delta wing of the same aspect ratio. It will be seen that although the experimental position of the aerodynamic centre does not agree with theory the agreement of variation with Mach number is remarkably good; the experimental position is about 3% behind the theoretical position throughout the speed range. It is interesting to note that the centre of area of the ogee is at 68.3% of the root chord, as compared with 66.66% for the delta. Thus the difference between the experimental curve for the ogee and the theoretical curve for the delta is about twice the difference of the centre of area of the two planforms. Finally, it should be noted that the aerodynamic centre for the ogee as given by slender body theory (attached flow) is at 64.8% of the root chord.

In the discussion of these results it should be noted that the wing tips were very flexible; the wing deflecting in such a manner as to reduce the loading at the trailing edge (the actual bending can be seen in the vapour screen photographs of Fig.12). Thus the aerodynamic centre of a rigid model would be further aft. Only one test was made to investigate this effect; at M = 1.3 the force tests were repeated at half the Reynolds number. The results at the low Reynolds number gave an aerodynamic centre position which was only a ¼% of c_o behind the high Reynolds number position. Thus at M = 1.3 the rigid model aerodynamic centre may be about 0.5% behind the quoted results. Since the highest model wing loading ** (for given incidence) occurred near M = 1.3 in this test series this shift of 0.5% is probably the maximum correction required throughout the speed range.

3.2 Drag

The variation of C_D with C_L is presented in Figs.13 and 14; the only point of interest in these curves is the dip in the drag curve near zero incidence. This drop in drag at low lift has been noted in other tests and is believed to be due to a region of laminar flow which occurs only at low lift, (suggesting that at low incidence the roughness was not completely fixing transistion). When the drag coefficient was plotted against C_L^2 it was found that the drag corresponding to incidences of 2° to about 6°

---

*All values of aerodynamic centre are found from slopes of the $C_m \sim C_L$ curves; this method is reasonably accurate if the curves are smooth, but extremely difficult where there are changes in slope, as in the present case at transonic speeds.

**The actual model wing loading at 6°, q C_L, varied from 0.2 lb/sq in. at M = 0.4 to 0.5 lb/sq in. at M = 1.2 dropping again to 0.4 lb/sq in. at M = 1.8.

varied almost linearly with C_L^2; this linear variation has been used to extrapolate to $C_L^2 = 0$ in order to obtain a $(C_{D_o})_T$ which is believed to be a fair value for a turbulent boundary layer at the test Reynolds number. The resultant values of $(C_{D_o})_T$ are plotted in Fig.15(a). At M = 0.4 the drag is close to the estimated skin-friction drag of the wing. With increase in speed the drag coefficient remains almost constant, in spite of a decrease in the skin-friction estimate, until M = 0.95 when it starts to increase reaching 0.0117 at M = 1.0. Above this Mach number the results are subject to severe wind tunnel interference effects and are not presented until the region of interference is past. At M = 1.3 the value of $(C_{D_o})_T$ is 0.0120 and above this Mach number it decreases steadily to 0.0101 at M = 1.8. Subtracting the estimated skin-friction drag the wave drag coefficient is 0.0042 at M = 1.3 and 0.0030 at M = 1.8. These values of the wave drag are compared in Fig.15(b) with the wave drag calculated by slender wing theory for the wing alone and for the wing plus body*. It will be seen that the measured drag is approximately 20% higher than the wing plus body theory values at M = 1.3 and 1.4 and 10% higher at M = 1.8. The reasons for this discrepancy are not fully understood; it should be pointed out, however, that the experimental results would be brought into excellent agreement with theory if the estimates of skin-friction drag were increased by 7%. The present estimate has been obtained from flat plate skin-friction drag; the Reynolds number was based on the wing mean chord and the wetted area was the actual wing surface area (2.12 × wing area). Previous results[12] have, however, suggested that this method may slightly overestimate the skin-friction drag and so the discrepancy may be greater than the results quoted above. More detailed investigation of this point must therefore be deferred until more reliable estimates of skin-friction drag are available

The drag due to lift results are plotted in Figs.16 and 17. Fig.16 shows the variation of $\pi A \{C_D - (C_{D_o})_T\}/C_L^2$ and $\pi A\alpha/C_L$ with Mach number at $C_L = 0.1$. Also plotted on this figure is the elliptic loading value of drag due to lift, 1.0, at subsonic speeds and the R.T. Jones lower bound, $1 + 2(\beta S_T/c_o)^2$ at supersonic speeds. Throughout the Mach number range the values of $\pi A \{C_D - (C_{D_o})_T\}/C_L^2$ lie below the experimental no leading edge suction values, $\pi A\alpha/C_L$. At subsonic speeds the actual amount below is about 33% of the difference between $\pi A\alpha/C_L$ and the theoretical minimum; at supersonic speeds $\pi A \{C_D - (C_{D_o})_T\}/C_L^2$ moves closer to $\pi A\alpha/C_L$, but even at M = 1.8 it is still about 26% of the difference below $\pi A\alpha/C_L$.

At supersonic speeds the values of $\pi A (C_D - C_{D_o})/C_L^2$ are in close agreement with values for delta wings of the same slenderness parameter as tested by Ormerod and Sprinks in the 8 ft tunnel at Bedford.

The variation of $\pi A\alpha/C_L$ and $\pi A \{C_D - (C_{D_o})_T\}/C_L^2$ with C_L at four representative Mach numbers are plotted in Fig.17. These plots show the decrease in the drag-due-to lift factor with increase in C_L, due to the non-linear lift of the vortices and also show that some leading edge thrust is achieved throughout the C_L range.

---

* The wing plus body drag was calculated by the methods of Ref.11; it should be noted that the theoretical wave drag for the wing plus body does not allow for base pressure, in these tests $(C_D)_{base}$ was at least 0.003 at supersonic speeds and so the total drag of the wing + body is greater than that of the wing alone.

4 CONCLUSIONS

Tests have been made throughout the Mach number range from M = 0.4 to M = 1.82 on a slender ogee wing to investigate the flow development and the longitudinal static stability.

The results show that at all speeds the flow separates from the leading edge at some positive incidences to form a pair of vortices above the wing. At subsonic speeds this separation occurs at very low incidence and the non-linear lift associated with the separated flow is almost independent of Mach number; at supersonic speeds the separations start to occur at progressively higher incidences with increase in Mach number and the non-linear lift drops off rapidly.

At M = 0.4 there is a slight decrease in stability with increase in lift, but this decrease is not present at higher Mach numbers. The overall shift in aerodynamic centre between M = 0.4 and M = 1.8 is about 6% of the root chord; most of this shift occurs below M = 1.0.

The zero lift wave drag of the model is higher than the theoretical value, but this may be due to the methods used to calculate the skin-friction drag. The drag due to lift is similar in magnitude to that obtained on a delta wing of the same aspect ratio.

LIST OF SYMBOLS

A	aspect ratio
$\bar{\bar{c}}$	aerodynamic mean chord
c_o	root chord
C_L	lift coefficient = lift/q S
C_m	pitching moment coefficient = moment/q $\bar{\bar{c}}$ S (moment about $\bar{\bar{c}}/4$)
C_D	drag coefficient = D/q S
$(C_{D_o})_T$	drag coefficient at zero lift with turbulent boundary layer
M	Mach number
q	free stream dynamic pressure
S	wing area
S_T	wing semi-span
α	wing incidence

LIST OF REFERENCES

Ref. No.	Author	Title, etc.
1	O'Hara, F. Squire, L.C. Haines, A.B.	An investigation of interference effects on similar models of different size in various transonic tunnels in the U.K. A.R.C. 21,094. February, 1959.
2	Mangler, K.W. Smith, J.H.B.	Calculation of the flow past slender delta wings with leading edge separations. Proc.Roy.Soc. Series A. Vol 251, pp.200-217, 1959.
3	Legendre, R.	Écoulement au voisinage de la pointe avant d'une aile a fate flèche aux incidences moyennes. La Recherche Aeronautique No.30, 1952, Nos.31 and 35, 1953. Translation in A.R.C.16,796.
4	Adams, Mac.C.	Leading edge separations from delta wings at supersonic speeds. Journal Aero Sciences Vol.20, p.430, 1953.
5	Edwards, R.H.	Leading edge separations from delta wings. Jour. Aero Sciences, Vol.21, p.134, 1954.
6	Brown, C.E. Michael, W.H.	Effect of leading edge separations on the lift of a delta wing. Jour. Aero Sciences, Vol.21, p.690, 1954.
7	Brown, C.E. Michael, W.H.	On slender delta wings with leading edge separations. NACA. Tech. Note No.3430. April, 1955.
8	Maskell, E.C.	Flow separations in three dimensions. A.R.C.18063. November, 1955.
9	Stanbrook, A. Squire, L.C.	Possible types of flow at swept leading edges. A.R.C. 21,464. April, 1959.
10	Squire, L.C. Jones, J.G. Stanbrook, A.	An experimental investigation of the characteristics of some plane and cambered 65° delta wings at Mach numbers from 0.7 to 2.0. A.R.C. 23,110. July, 1961.
11	Lighthill, M.J.	The wave drag at zero lift of slender delta wings and similar configurations. Jour. Fluid Mechanics, Vol.1, p.337, 1956.
12	Squire, L.C.	An experimental investigation at supersonic speeds of the characteristics of two gothic wings; one plane and one cambered. A.R.C. R & M.3211. May, 1959.

TABLE 1

Aerodynamic coefficients

M	α	C_L	C_m	C_D
0.4	-1.99	-0.051	+0.0069	+0.0104
	-1.02	-0.021	+0.0016	+0.0091
	-0	+0.006	-0.0029	+0.0079
	+1.02	+0.033	-0.0067	+0.0094
	+2.04	+0.067	-0.0132	+0.0112
	+3.07	+0.101	-0.0189	+0.0139
	+4.10	+0.141	-0.0265	+0.0184
	+5.13	+0.180	-0.0330	+0.0240
	+6.16	+0.220	-0.0399	+0.0310
	+7.19	+0.262	-0.0465	+0.0398
	+8.22	+0.307	-0.0537	+0.0505
	+9.26	+0.353	-0.0610	+0.0630
	+10.30	+0.401	-0.0688	+0.0778
	+11.34	+0.449	-0.0768	+0.0941
	+12.38	+0.496	-0.0838	+0.1123
	+13.42	+0.548	-0.0919	+0.1331
0.7	-1.97	-0.054	+0.0084	+0.0105
	-1.03	-0.022	+0.0023	+0.0089
	+0	+0.005	-0.0021	+0.0074
	+1.04	+0.035	-0.0070	+0.0090
	+2.08	+0.068	-0.0129	+0.0109
	+3.12	+0.105	-0.0201	+0.0138
	+4.16	+0.147	-0.0280	+0.0185
	+5.21	+0.190	-0.0362	+0.0247
	+6.27	+0.233	-0.0437	+0.0327
	+7.32	+0.277	-0.0519	+0.0420
	+8.38	+0.326	-0.0605	+0.0537
	+9.43	+0.373	-0.0690	+0.0672
	+10.50	+0.423	-0.0779	+0.0829
	+11.55	+0.469	-0.0859	+0.0998
	+12.62	+0.522	-0.0955	+0.1201
	+13.68	+0.569	-0.1039	+0.1411
0.8	-1.98	-0.059	+0.0100	+0.0105
	-1.04	-0.025	+0.0033	+0.0088
	+0	+0.003	-0.0012	+0.0073
	+1.04	+0.033	-0.0064	+0.0091
	+2.09	+0.071	-0.0140	+0.0112
	+3.13	+0.107	-0.0212	+0.0140
	+4.18	+0.151	-0.0294	+0.0188
	+5.24	+0.195	-0.0378	+0.0254
	+6.30	+0.241	-0.0464	+0.0335
	+7.35	+0.286	-0.0555	+0.0432
	+8.42	+0.337	-0.0654	+0.0557
	+9.48	+0.387	-0.0748	+0.0698
	+10.55	+0.438	-0.0852	+0.0862
	+11.62	+0.490	-0.0955	+0.1050
	+12.68	+0.541	-0.1056	+0.1255
	+13.75	+0.594	-0.1162	+0.1488

TABLE 1 (Contd)

M	α	C_L	C_m	C_D
0.9	-1.98	-0.060	+0.0105	+0.0105
	-1.04	-0.025	+0.0033	+0.0090
	+0	+0.006	-0.0027	+0.0074
	+1.05	+0.038	-0.0080	+0.0092
	+2.09	+0.075	-0.0158	+0.0113
	+3.14	+0.114	-0.0236	+0.0145
	+4.20	+0.159	-0.0331	+0.0197
	+5.26	+0.207	-0.0430	+0.0265
	+6.32	+0.256	-0.0536	+0.0356
	+7.38	+0.305	-0.0639	+0.0463
	+8.45	+0.355	-0.0750	+0.0591
	+9.52	+0.410	-0.0874	+0.0745
	+10.58	+0.459	-0.0984	+0.0912
	+11.65	+0.515	-0.1110	+0.1112
	+12.71	+0.564	-0.1220	+0.1320
	+13.78	+0.619	-0.1352	+0.1564
0.94	-1.99	-0.062	+0.0109	+0.0109
	-1.04	-0.027	+0.0037	+0.0092
	+0	+0.006	-0.0026	+0.0076
	+1.05	+0.038	-0.0081	+0.0093
	+2.09	+0.075	-0.0161	+0.0116
	+3.15	+0.117	-0.0250	+0.0149
	+4.21	+0.164	-0.0351	+0.0203
	+5.26	+0.210	-0.0453	+0.0272
	+6.32	+0.260	-0.0569	+0.0363
	+7.39	+0.314	-0.0693	+0.0480
	+8.45	+0.367	-0.0822	+0.0613
	+9.51	+0.421	-0.0961	+0.0771
	+10.57	+0.473	-0.1084	+0.0947
	+11.63	+0.526	-0.1224	+0.1143
	+12.69	+0.586	-0.1408	+0.1379
	+13.75	+0.642	-0.1565	+0.1628
0.98	-1.99	-0.065	+0.0127	+0.0121
	-1.05	-0.030	+0.0046	+0.0105
	+0	+0.004	-0.0015	+0.0085
	+1.05	+0.036	-0.0075	+0.0104
	+2.09	+0.075	-0.0170	+0.0124
	+3.14	+0.119	-0.0275	+0.0159
	+4.20	+0.169	-0.0400	+0.0216
	+5.25	+0.222	-0.0548	+0.0296
	+6.31	+0.268	-0.0656	+0.0387
	+7.36	+0.326	-0.0826	+0.0512
	+8.42	+0.377	-0.0954	+0.0647
	+9.48	+0.431	-0.1097	+0.0806
	+10.54	+0.481	-0.1225	+0.0979
	+11.60	+0.531	-0.1350	+0.1173
	+12.66	+0.580	-0.1473	+0.1385
	+13.73	+0.632	-0.1613	+0.1630

TABLE 1 (Contd.)

M	α	C_L	C_m	C_D
1.00	-1.98	-0.071	+0.0169	+0.0134
	-1.04	-0.033	+0.0071	+0.0122
	-0	+0.004	-0.0027	+0.0102
	+1.04	+0.039	-0.0100	+0.0121
	+2.09	+0.080	-0.0200	+0.0144
	+3.14	+0.125	-0.0309	+0.0178
	-4.19	+0.172	-0.0434	+0.0235
	+5.24	+0.220	-0.0557	+0.0308
	+6.30	+0.273	-0.0691	+0.0400
	+7.36	+0.325	-0.0827	+0.0519
	+8.42	+0.377	-0.0963	+0.0649
	+9.48	+0.428	-0.1092	+0.0804
	+10.54	+0.480	-0.1231	+0.0987
	+11.60	+0.529	-0.1357	+0.1174
	+12.66	+0.578	-0.1481	+0.1383
	+13.72	+0.626	-0.1604	+0.1612
1.25	-1.97	-0.067	+0.0182	
	-1.04	-0.031	+0.0083	
	+0.01	+0.002		
	+1.05	+0.036	-0.0090	
	+2.09	+0.075	-0.0194	
	+3.13	+0.114	-0.0298	
	+4.19	+0.157	-0.0412	
	+5.23	+0.200	-0.0529	
	+6.29	+0.245	-0.0645	
	+7.34	+0.288	-0.0762	
	+8.40	+0.332	-0.0875	
	+9.45	+0.379	-0.1002	
	+10.51	+0.421	-0.1113	
	+11.56	+0.463	-0.1218	
	+12.62	+0.505	-0.1328	
	+13.68	+0.546	-0.1437	
1.32	-2.08	-0.075	+0.0222	+0.0142
	-1.03	-0.037	+0.0118	+0.0123
	+0.01	-0.005	+0.0032	+0.0118
	+1.05	+0.034	-0.0070	+0.0126
	+2.09	+0.064	-0.0149	+0.0141
	+3.14	+0.104	-0.0253	+0.0169
	+4.18	+0.146	-0.0367	+0.0214
	+5.23	+0.188	-0.0476	+0.0276
	+6.28	+0.230	-0.0588	+0.0352
	+7.34	+0.273	-0.0703	+0.0447
	+8.39	+0.316	-0.0817	+0.0558
	+9.44	+0.358	-0.0929	+0.0686
	+10.50	+0.401	-0.1040	+0.0829

TABLE 1 (Contd.)

M	α	C_L	C_m	C_D
1.42	-2.07	-0.066	+0.0182	+0.0136
	-1.03	-0.031	+0.0087	+0.0120
	+0.01	+0.003		+0.0113
	+1.05	+0.036	-0.0089	+0.0124
	+2.09	+0.071	-0.0181	+0.0139
	+3.13	+0.109	-0.0283	+0.0168
	+4.18	+0.149	-0.0389	+0.0214
	+5.23	+0.189	-0.0498	+0.0273
	+6.28	+0.230	-0.0606	+0.0348
	+7.33	+0.270	-0.0713	+0.0441
	+8.38	+0.311	-0.0821	+0.0547
	+9.43	+0.352	-0.0930	+0.0670
	+10.48	+0.390	-0.1030	+0.0805
1.61	-2.07	-0.053	+0.0130	+0.0124
	-1.03	-0.022	+0.0050	+0.0107
	+0.01	+0.010	-0.0036	+0.0103
	+1.04	+0.041	-0.0117	+0.0114
	+2.08	+0.074	-0.0207	+0.0134
	+3.13	+0.109	-0.0300	+0.0163
	+4.17	+0.144	-0.0395	+0.0205
	+5.21	+0.181	-0.0491	+0.0261
	+6.26	+0.217	-0.0586	+0.0330
	+7.31	+0.254	-0.0682	+0.0416
	+8.36	+0.290	-0.0778	+0.0515
	+9.40	+0.325	-0.0871	+0.0625
	+10.45	+0.360	-0.0957	+0.0747
1.82	-2.07	-0.058	+0.0149	+0.0116
	-1.04	-0.029	+0.0071	+0.0095
		+0.002	-0.0011	+0.0088
	+1.04	+0.031	-0.0082	+0.0100
	+2.07	+0.061	-0.0162	+0.0121
	+3.11	+0.093	-0.0246	+0.0148
	+4.15	+0.126	-0.0336	+0.0187
	+5.20	+0.160	-0.0425	+0.0239
	+6.24	+0.193	-0.0509	+0.0301
	+7.28	+0.226	-0.0595	+0.0377
	+8.32	+0.258	-0.0676	+0.0464
	+9.37	+0.291	-0.0759	+0.0565
	+10.41	+0.323	-0.0842	+0.0679

WT.2078.C.P.585.K3 - Printed in England

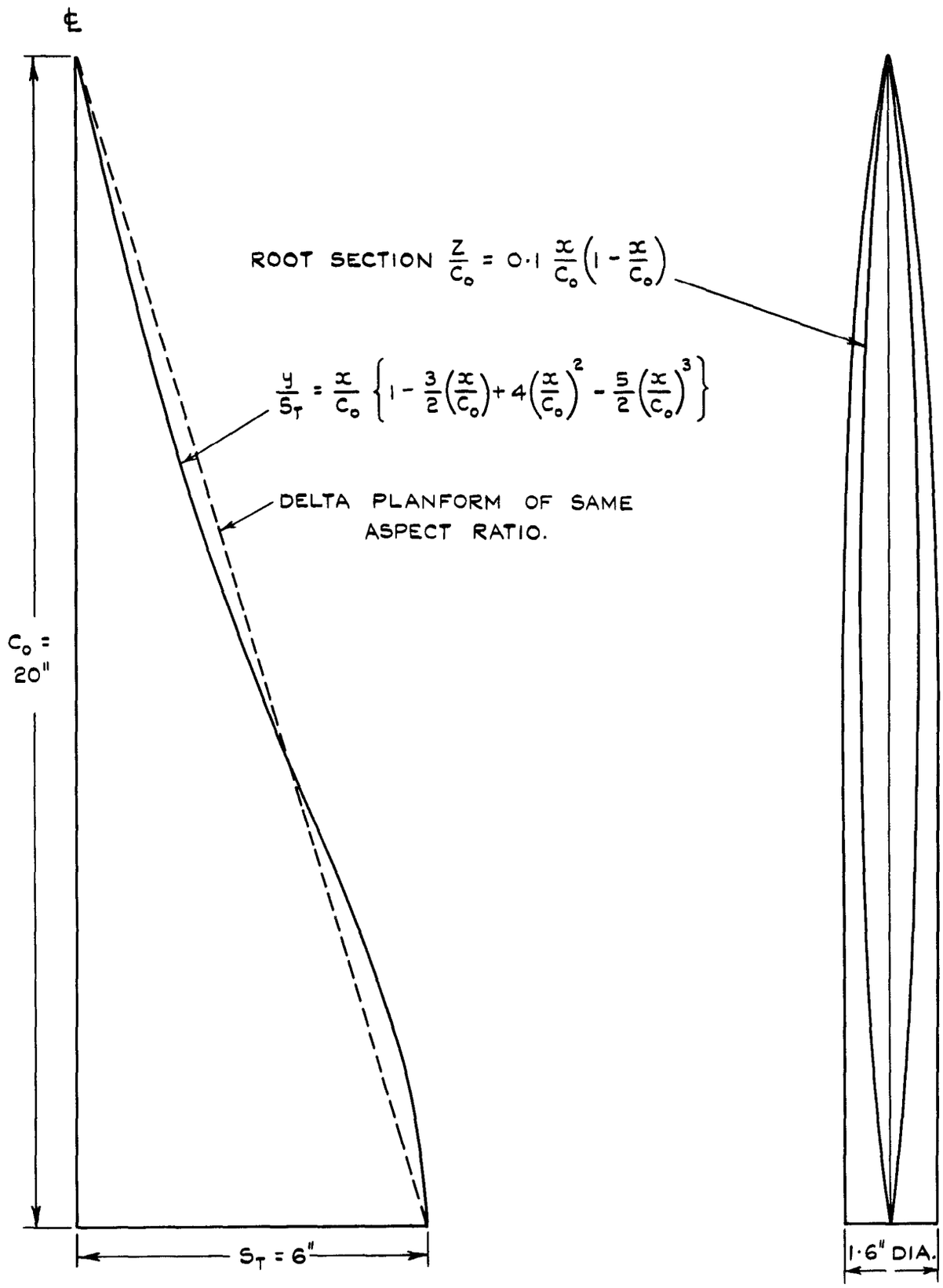

WING AREA = $S_T C_0$ = 120 SQ. IN.

ASPECT RATIO = 1·2

WING SECTION : DIAMOND SECTIONS NORMAL TO CHORD.

FIG. 1. DETAILS OF THE MODEL.

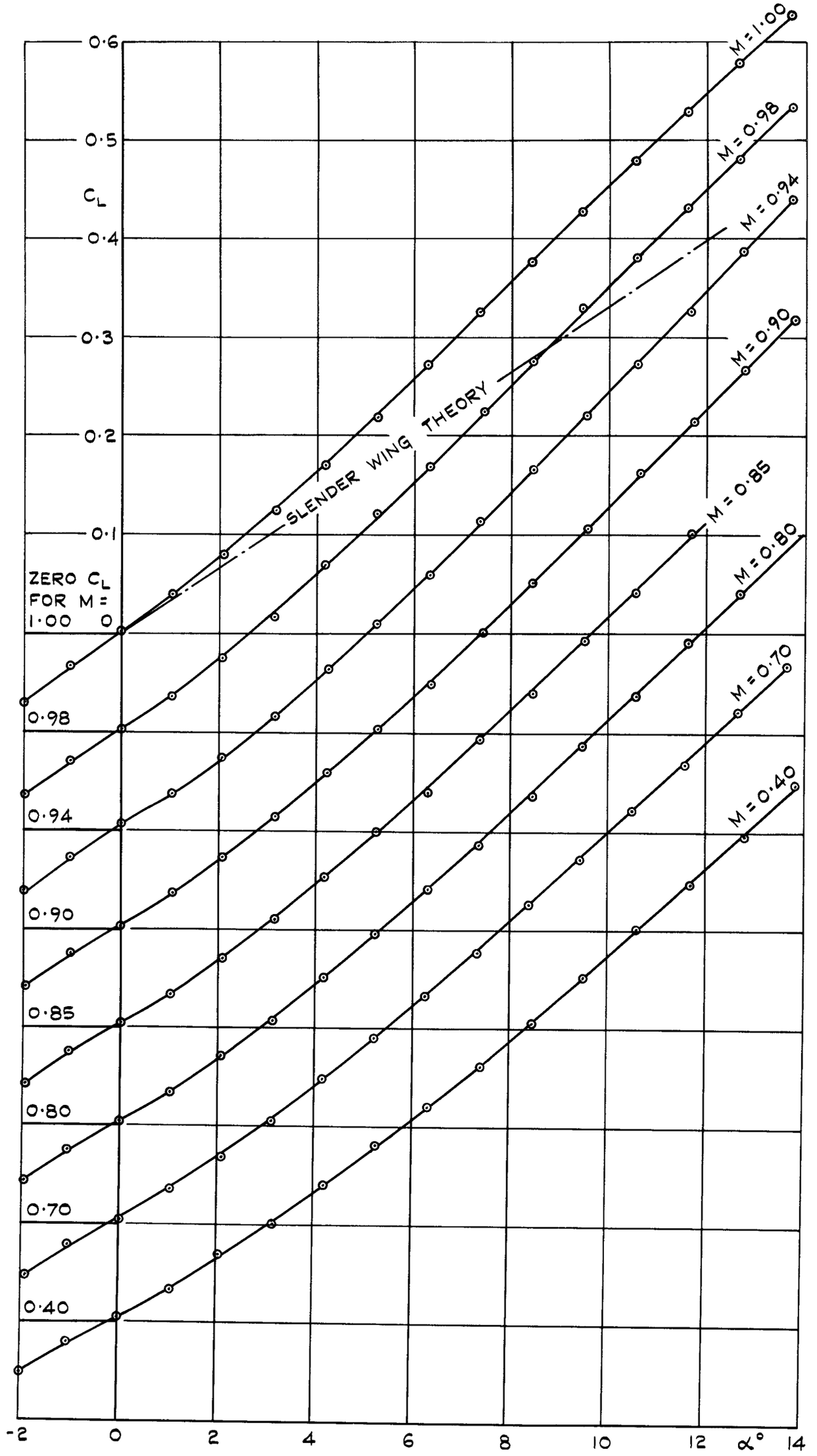

FIG. 2. VARIATION OF C_L WITH α : M = 0·4 TO M = 1·00.

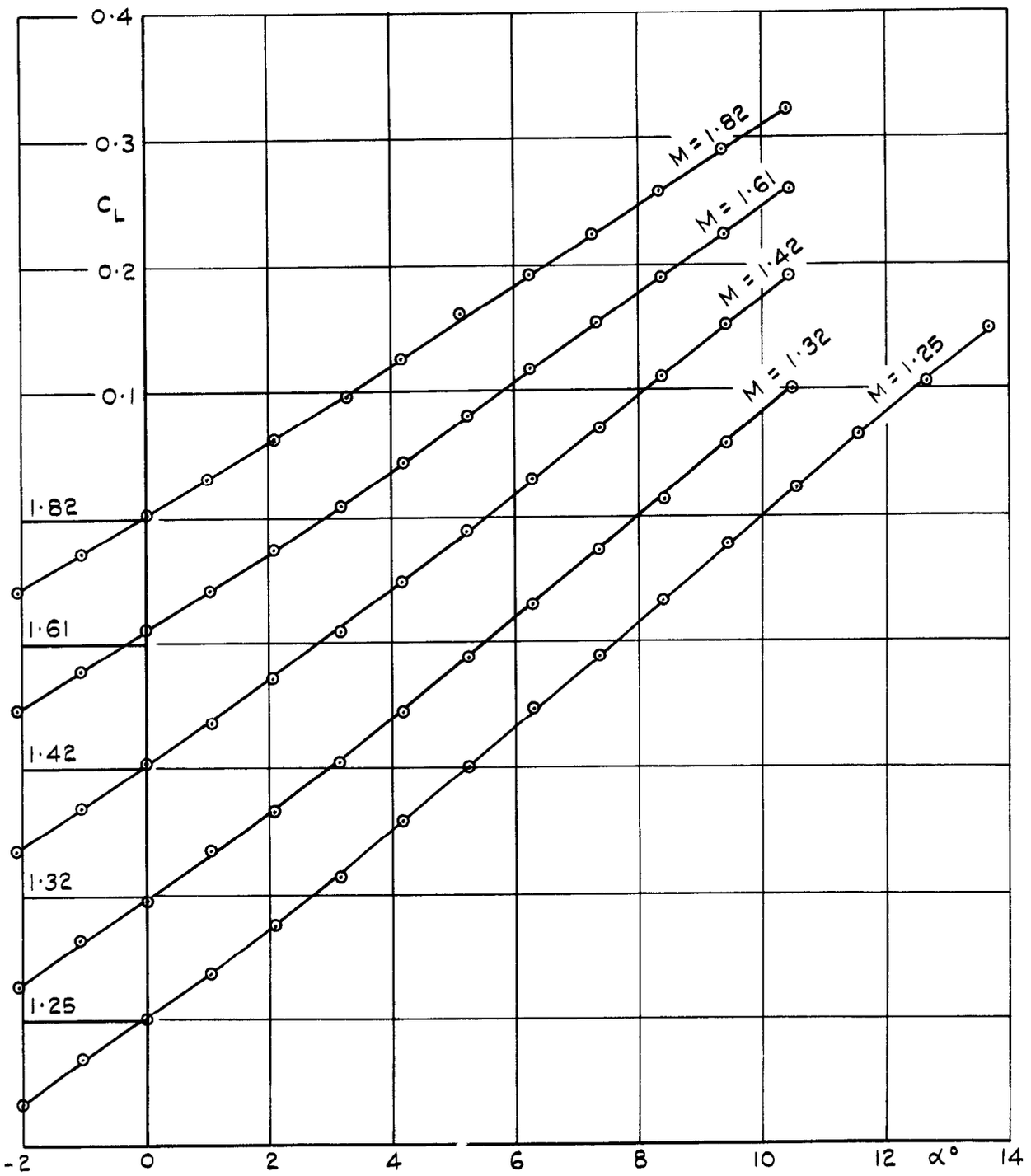

FIG. 3. VARIATION OF C_L WITH α:
M = 1·25 TO M = 1·82.

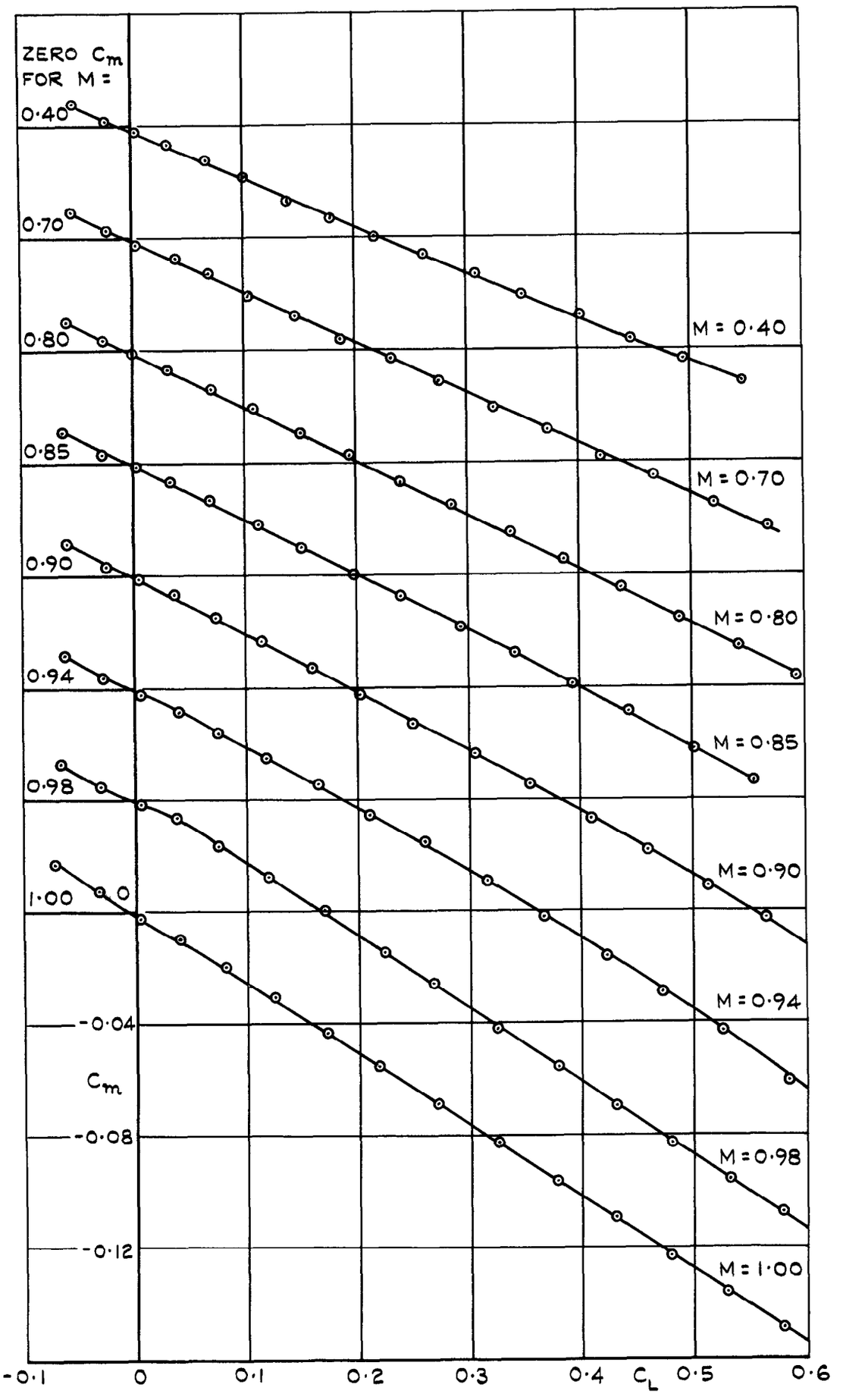

FIG. 4. VARIATION OF C_m WITH C_L: M = 0·4 TO M = 1·00.

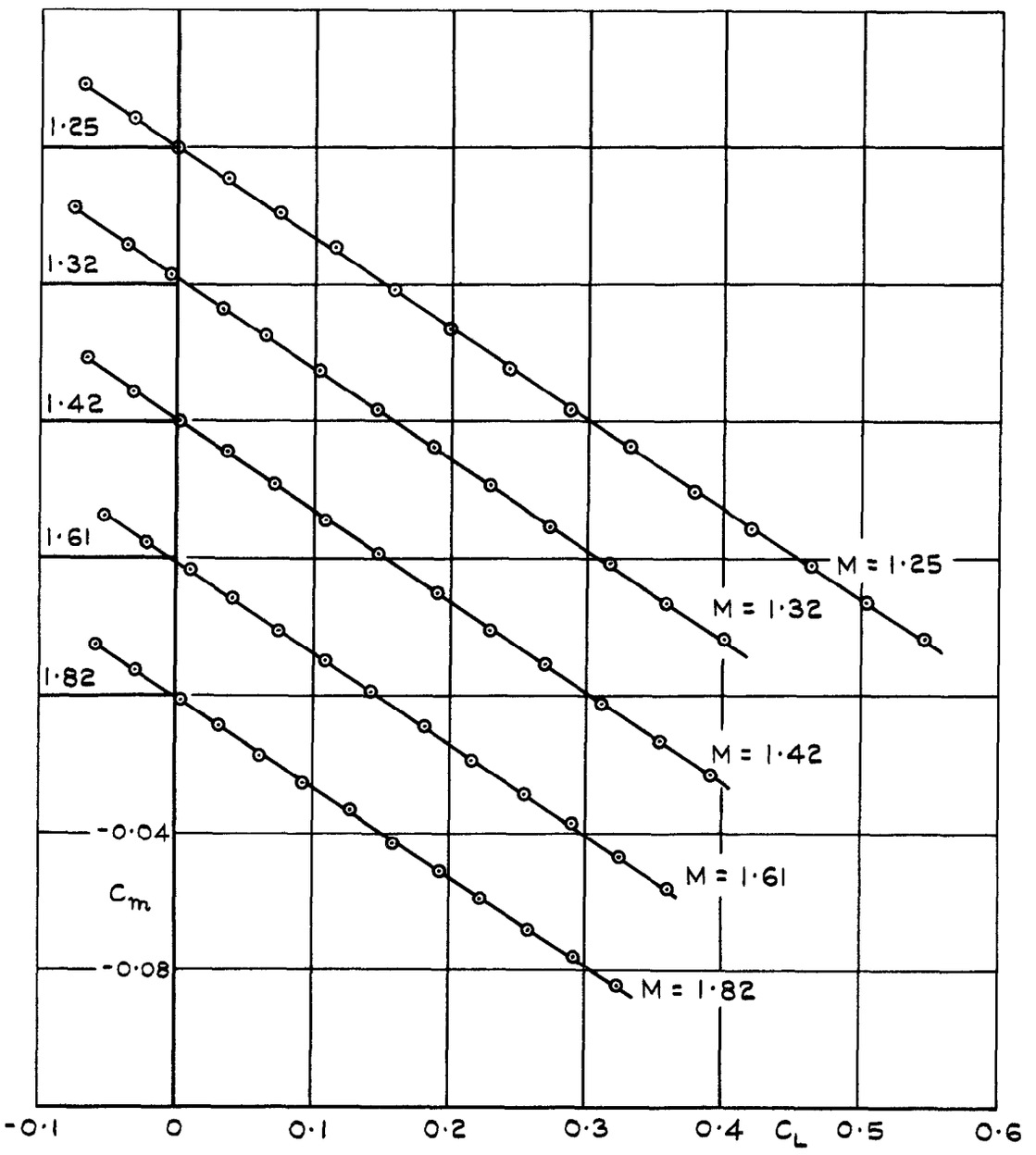

FIG. 5. VARIATION OF C_m WITH C_L: M = 1·25 TO M = 1·82.

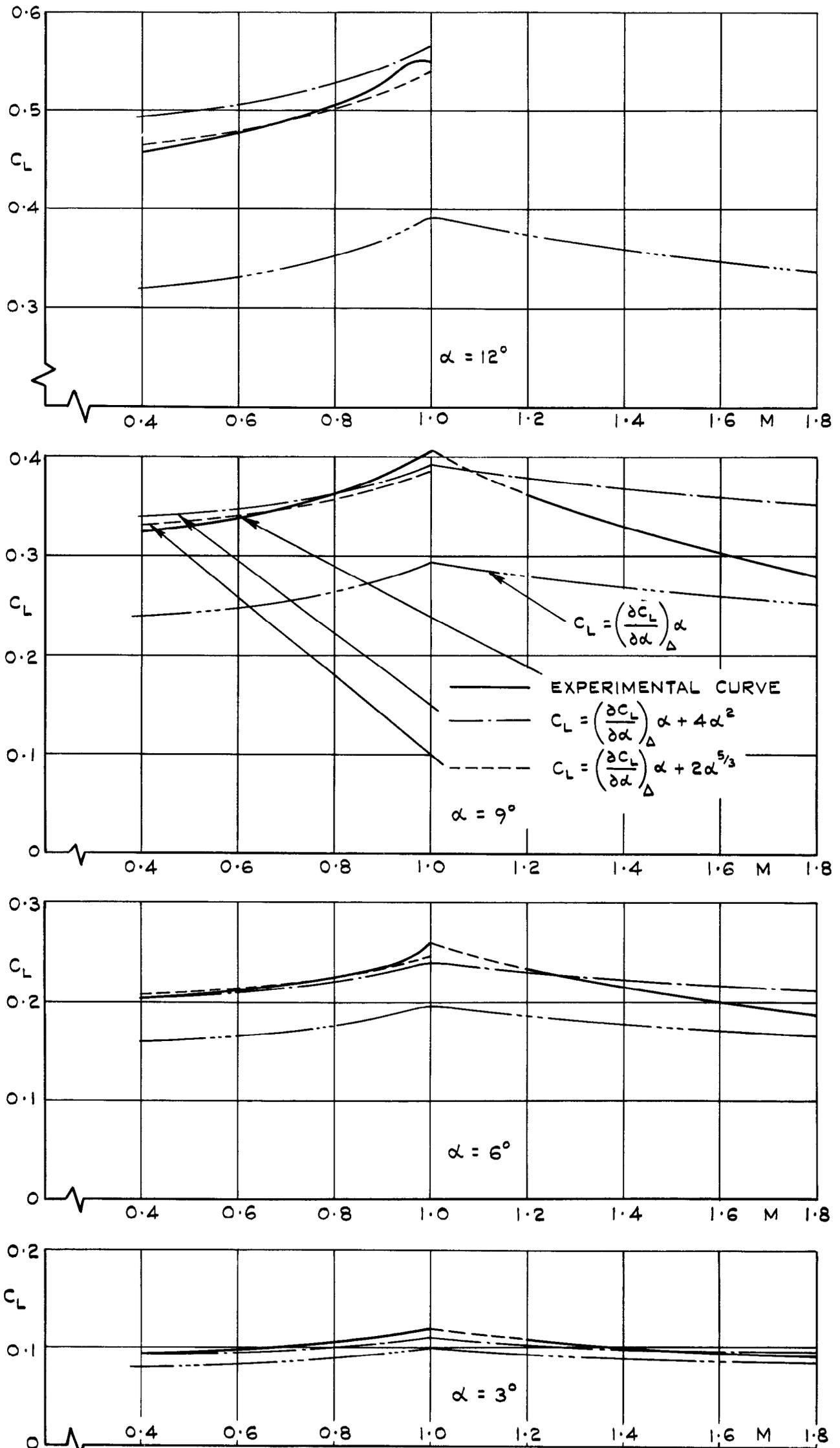

FIG. 6. VARIATION OF C_L WITH MACH NUMBER AT CONSTANT INCIDENCE.

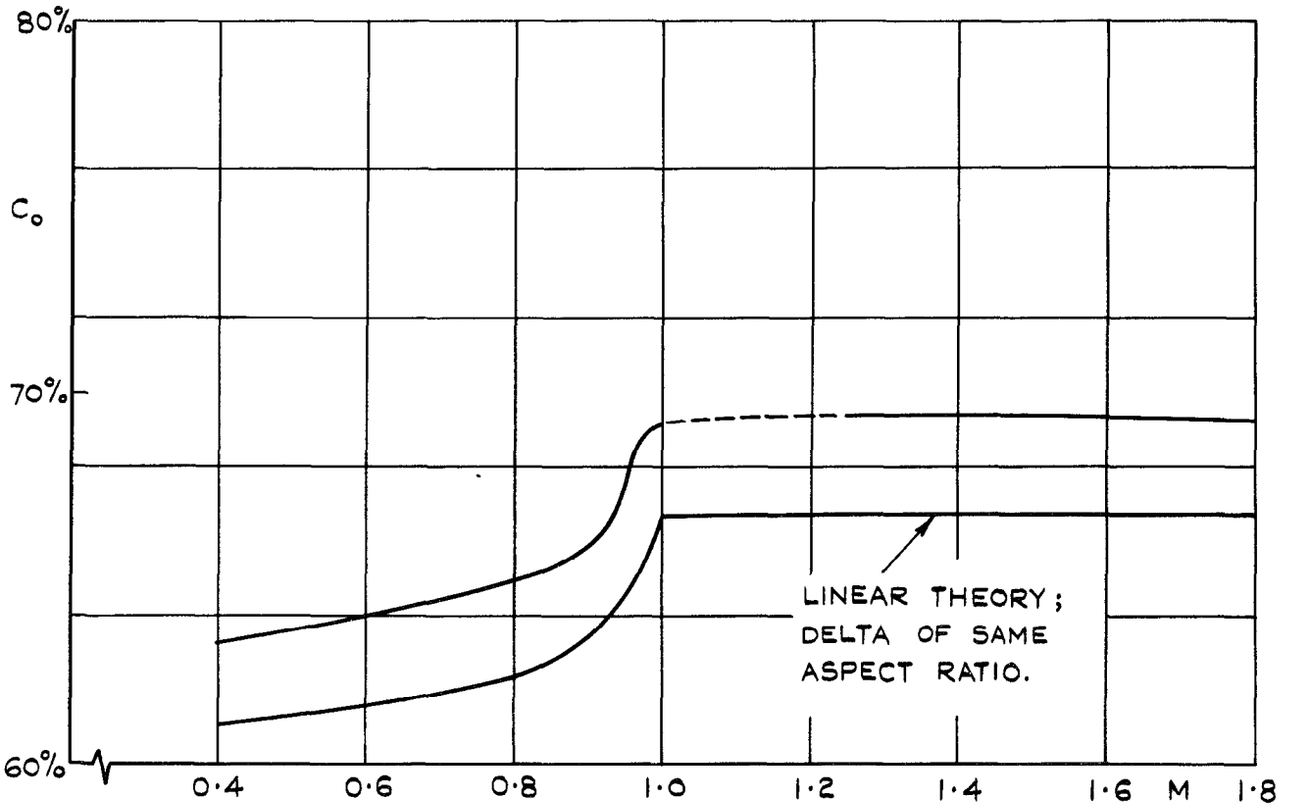

FIG. 7. POSITION OF AERODYNAMIC CENTRE ($C_L = 0 \cdot 1$) ON ROOT CHORD.

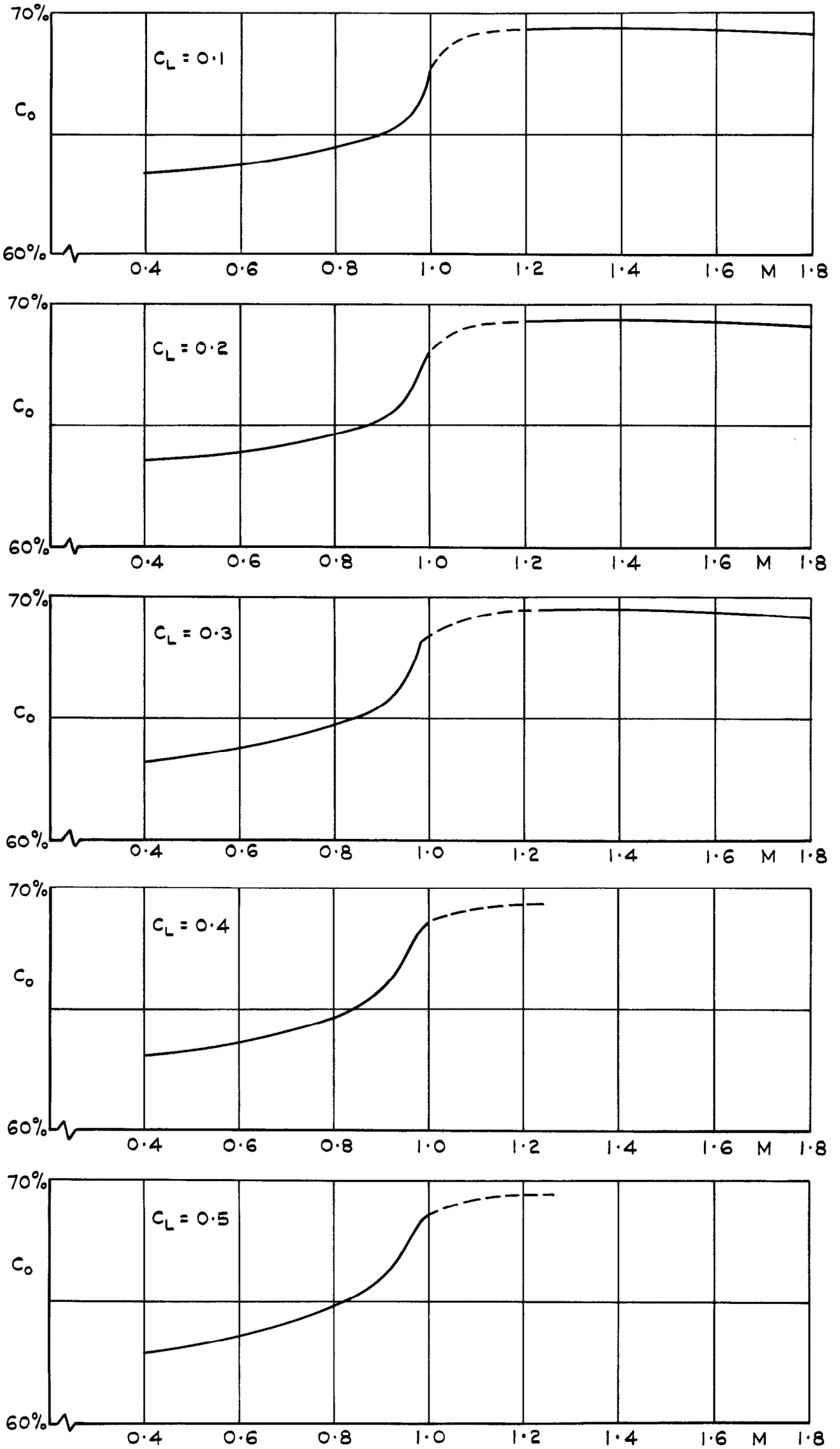

FIG. 8. POSITION OF CENTRE OF PRESSURE.

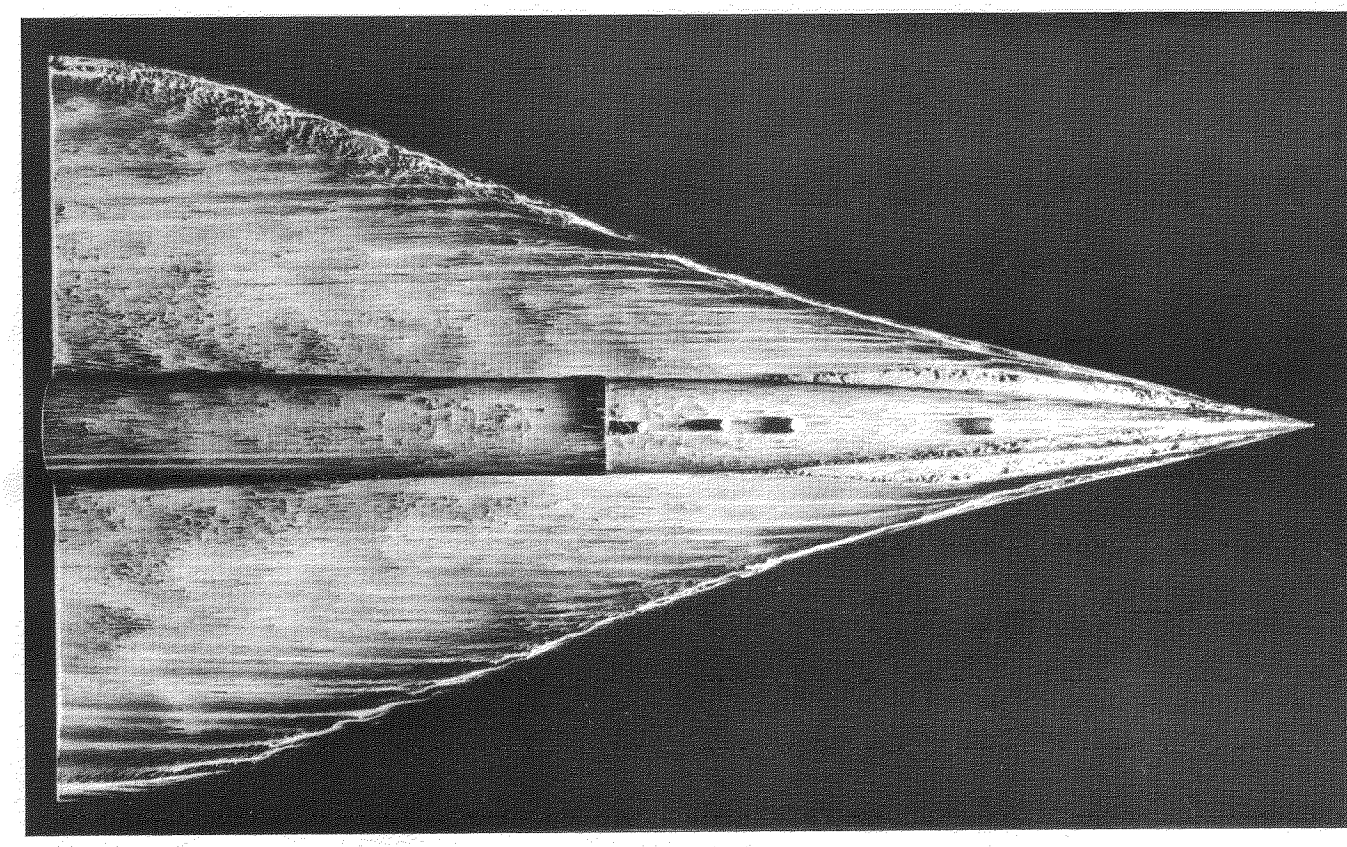

M = 1.61

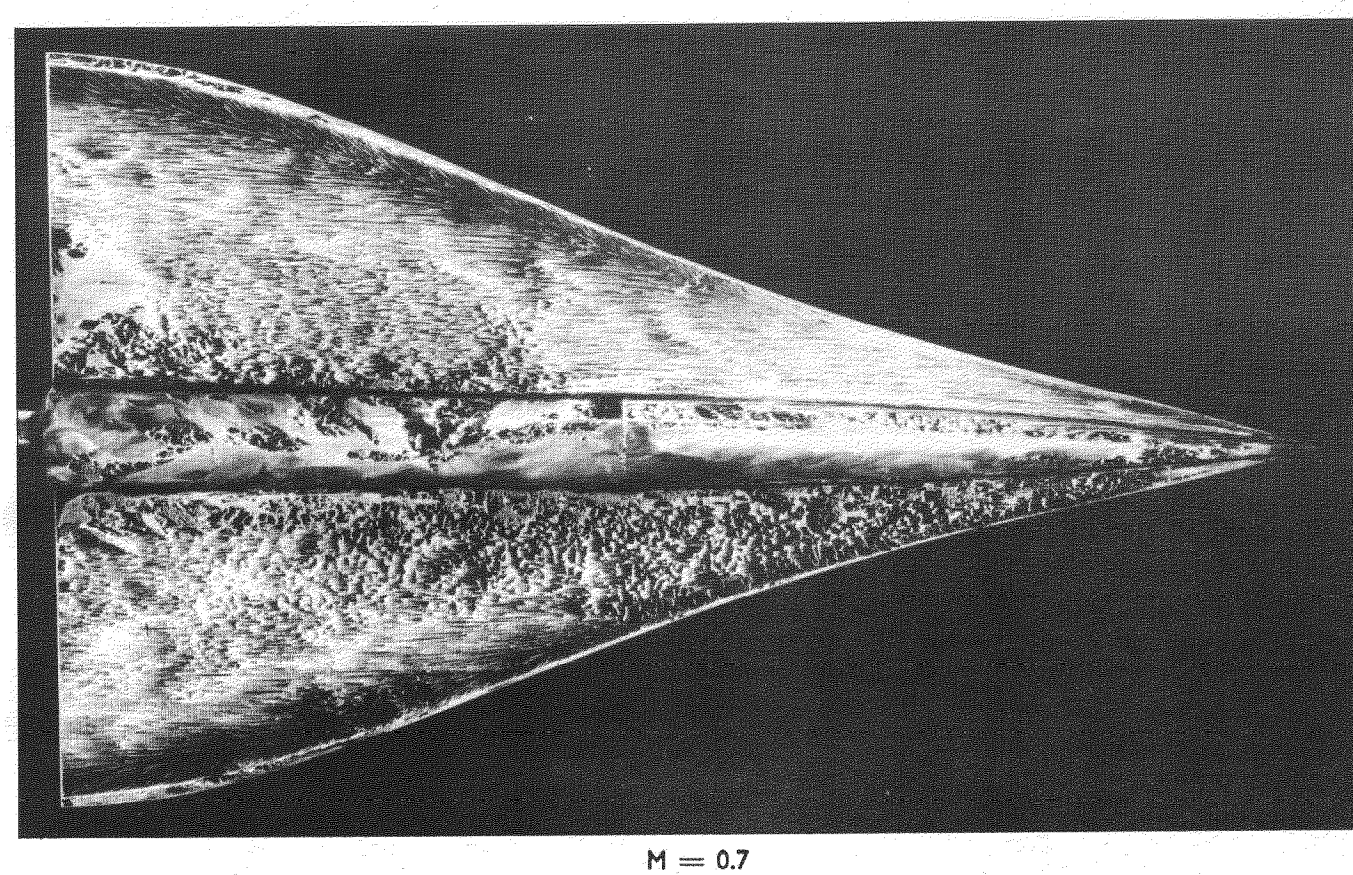

M = 0.7

FIG.9. OIL FLOW PATTERNS AT APPROXIMATELY 2° INCIDENCE

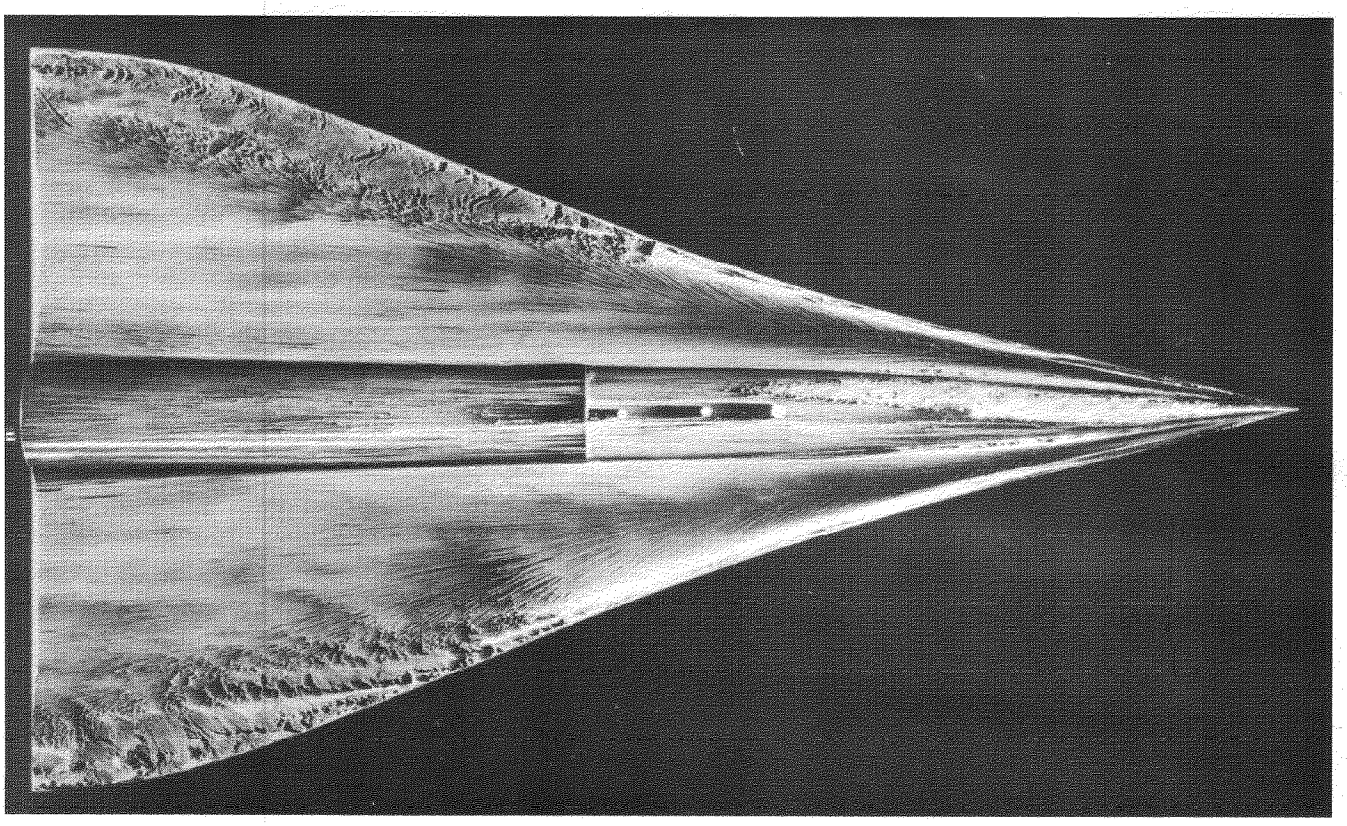

M = 1.61

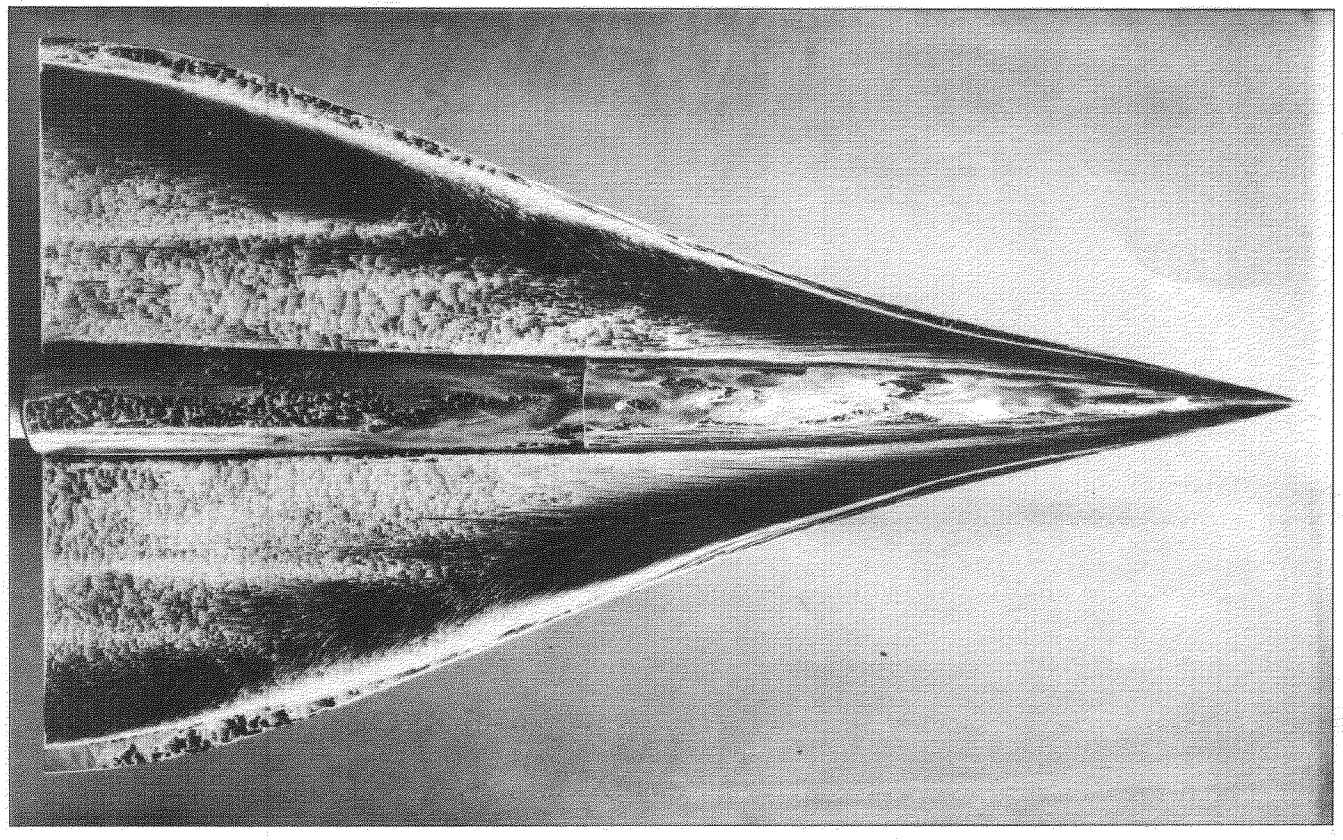

M = 0.7

FIG.10. OIL FLOW PATTERNS AT APPROXIMATELY 4° INCIDENCE

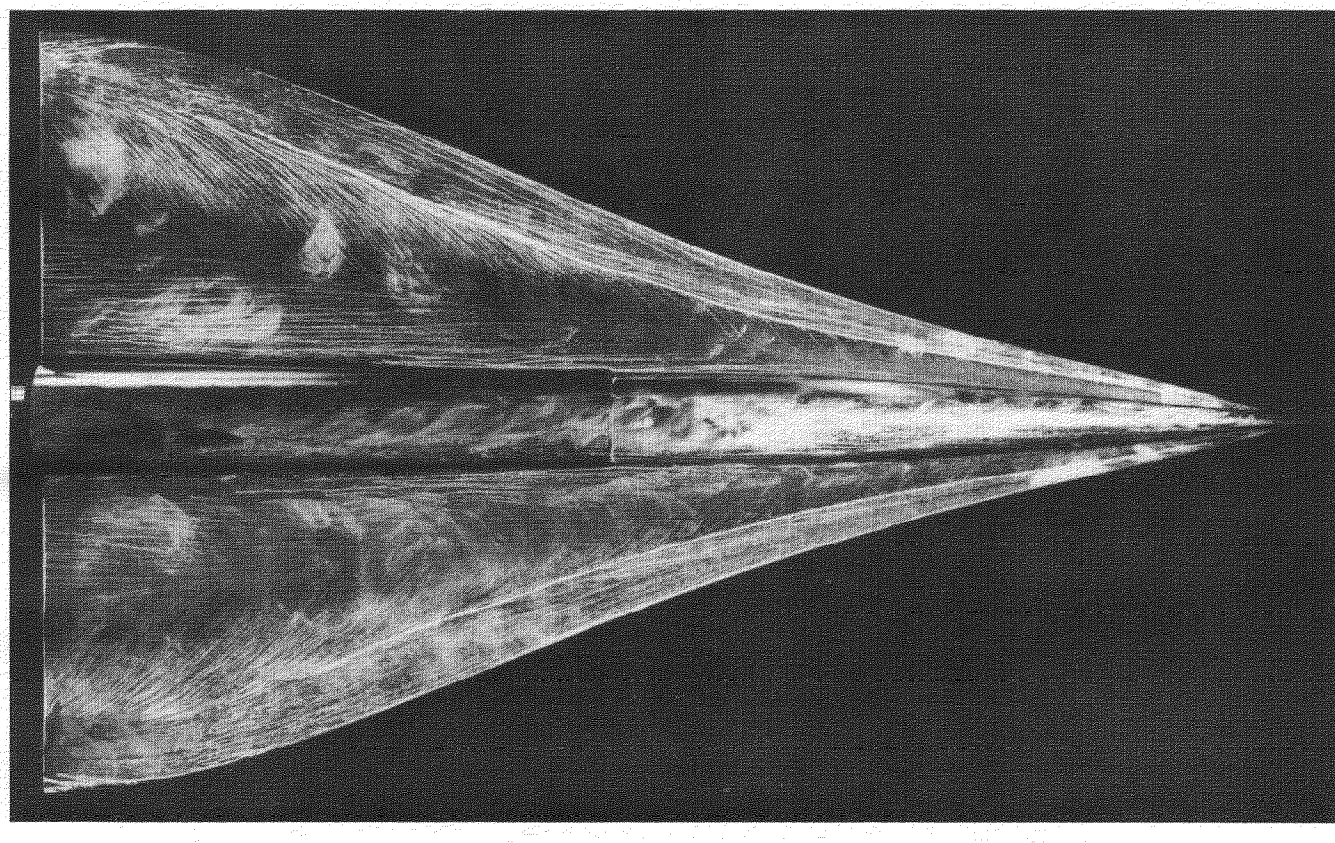

M = 1.61

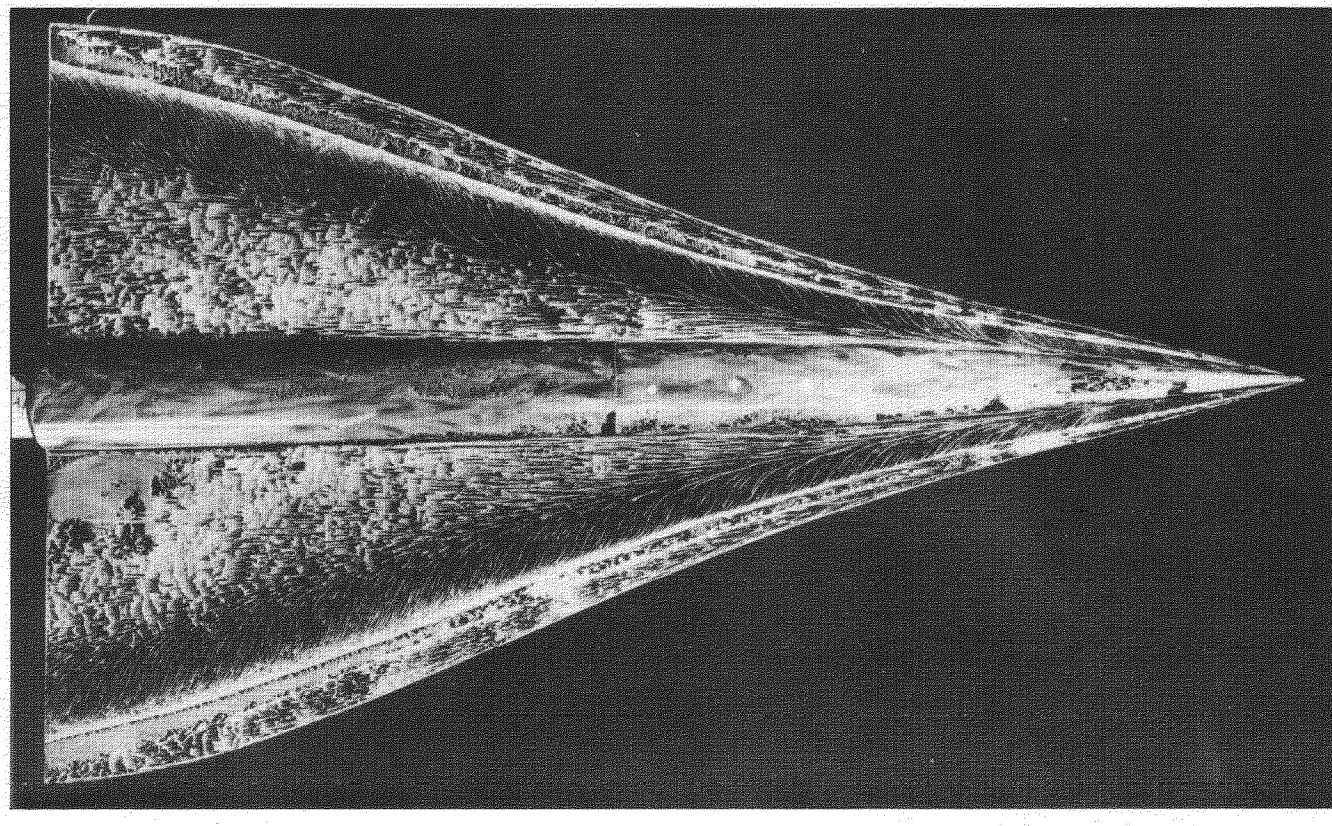

M = 0.7

FIG.11. OIL FLOW PATTERNS AT APPROXIMATELY 8° INCIDENCE

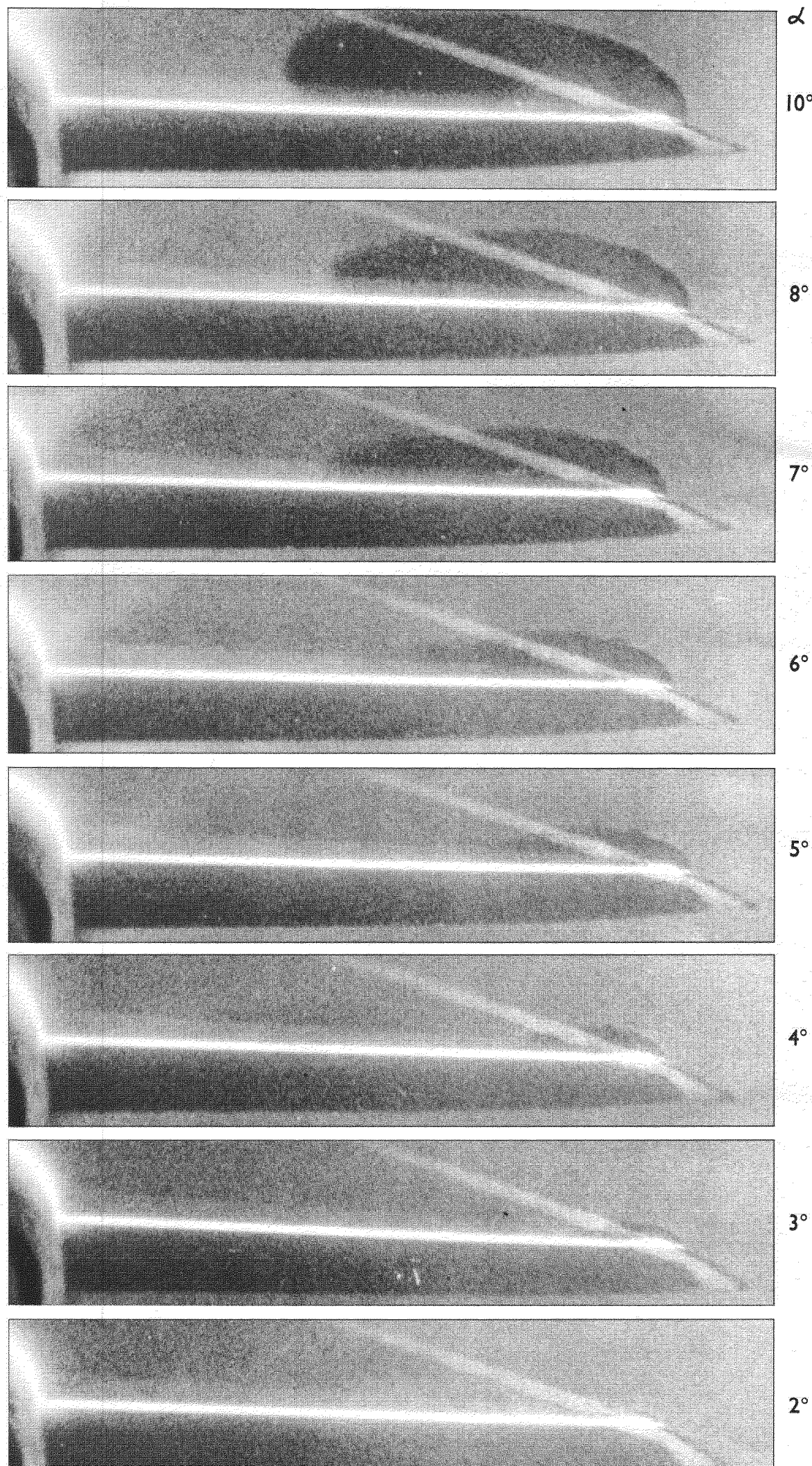
α
10°
8°
7°
6°
5°
4°
3°
2°

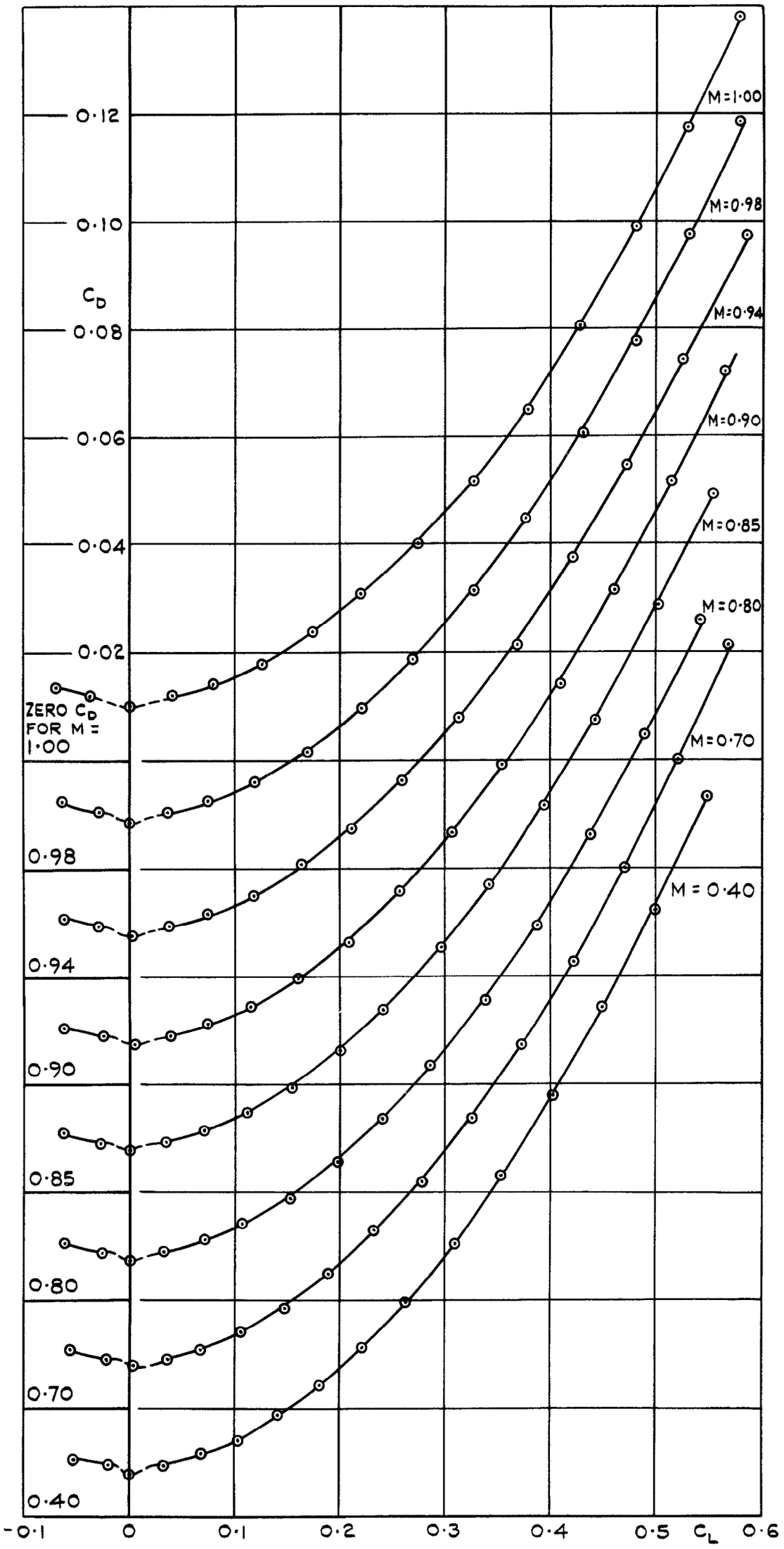

FIG. 13. VARIATION OF C_D WITH C_L: M = 0·4 TO M = 1·00.

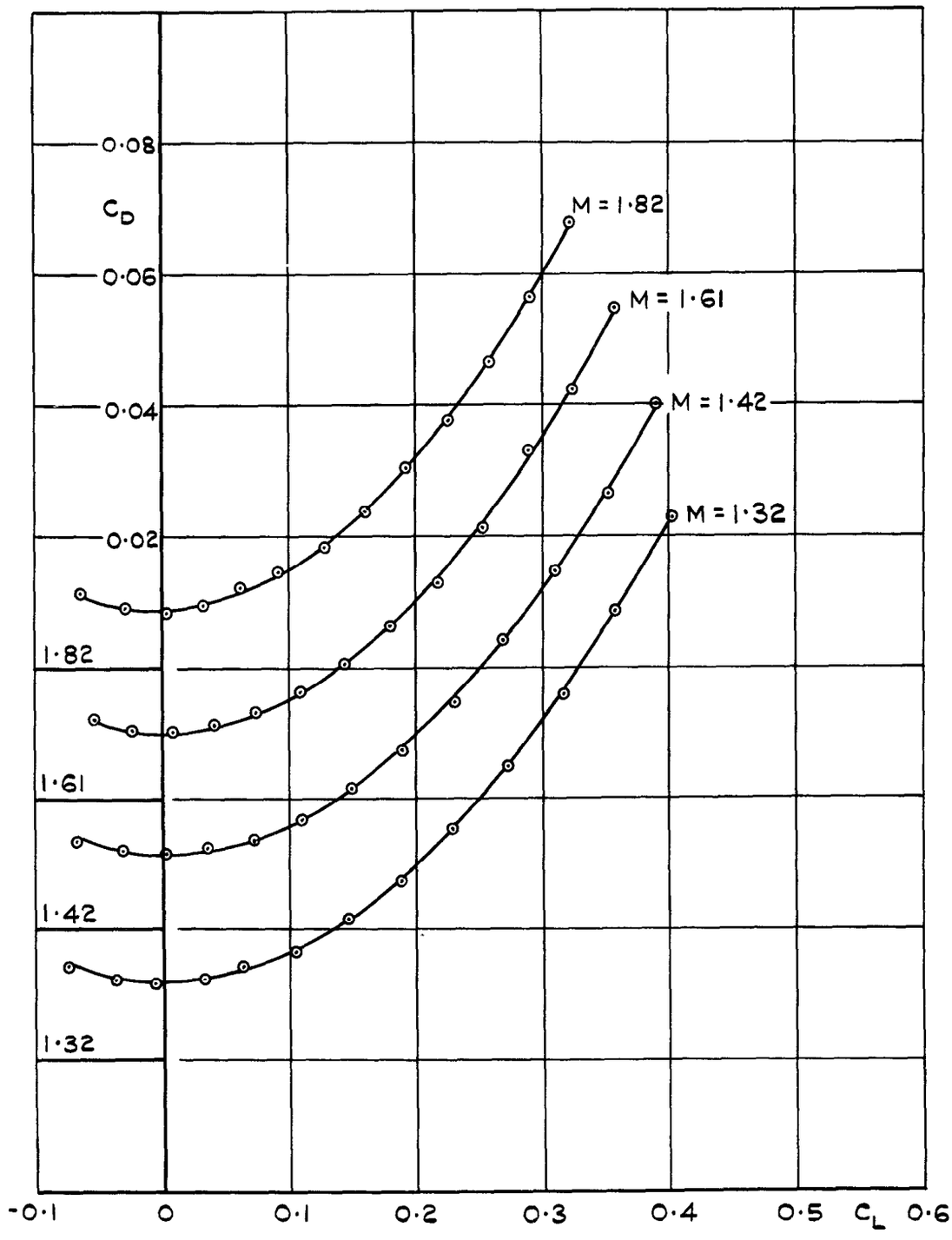

FIG. 14. VARIATION OF C_D WITH C_L: M = 1·32 TO M = 1·82.

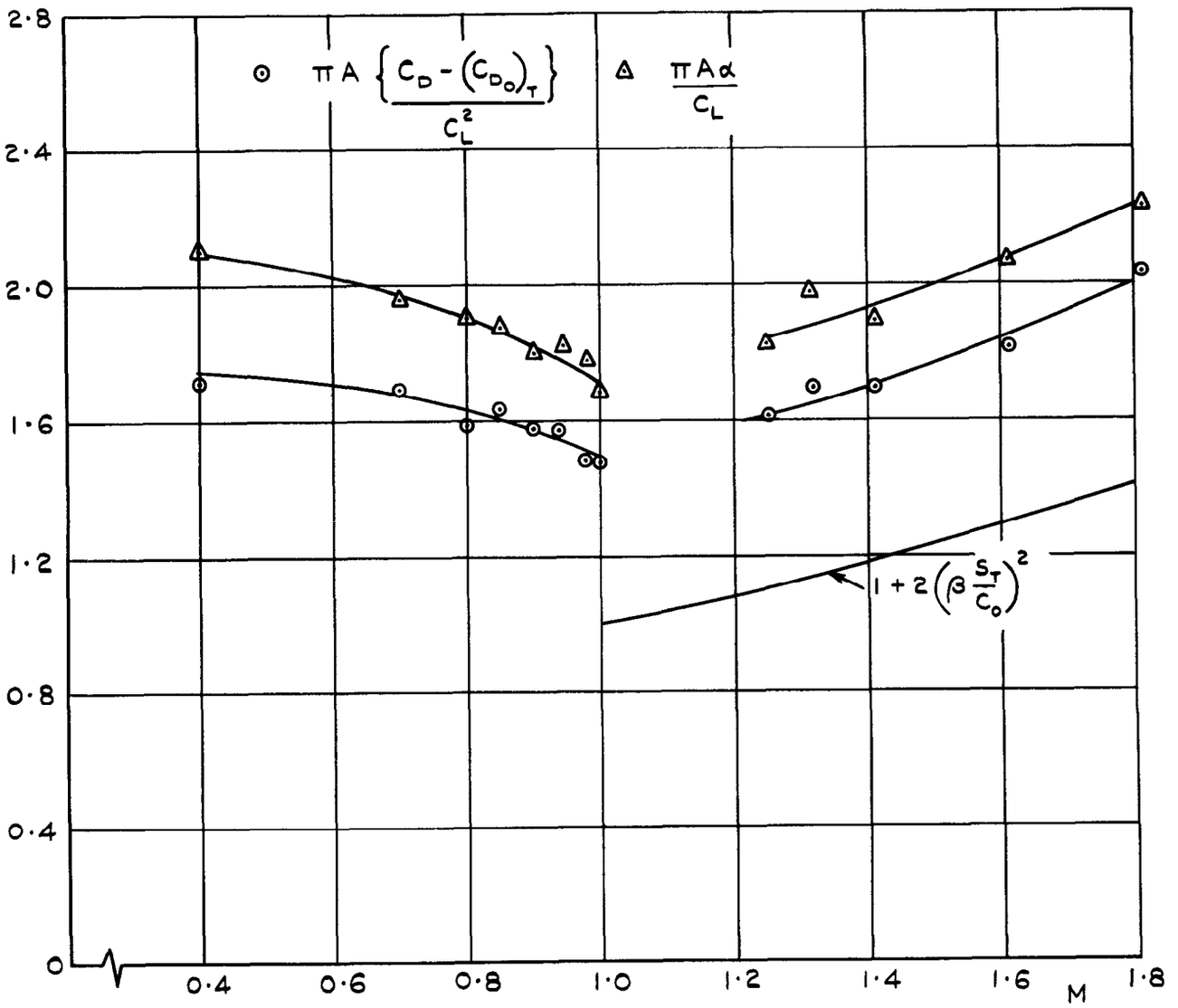

FIG. 16. VARIATION OF INDUCED DRAG FACTOR ($C_L = 0 \cdot 1$) WITH MACH NUMBER.

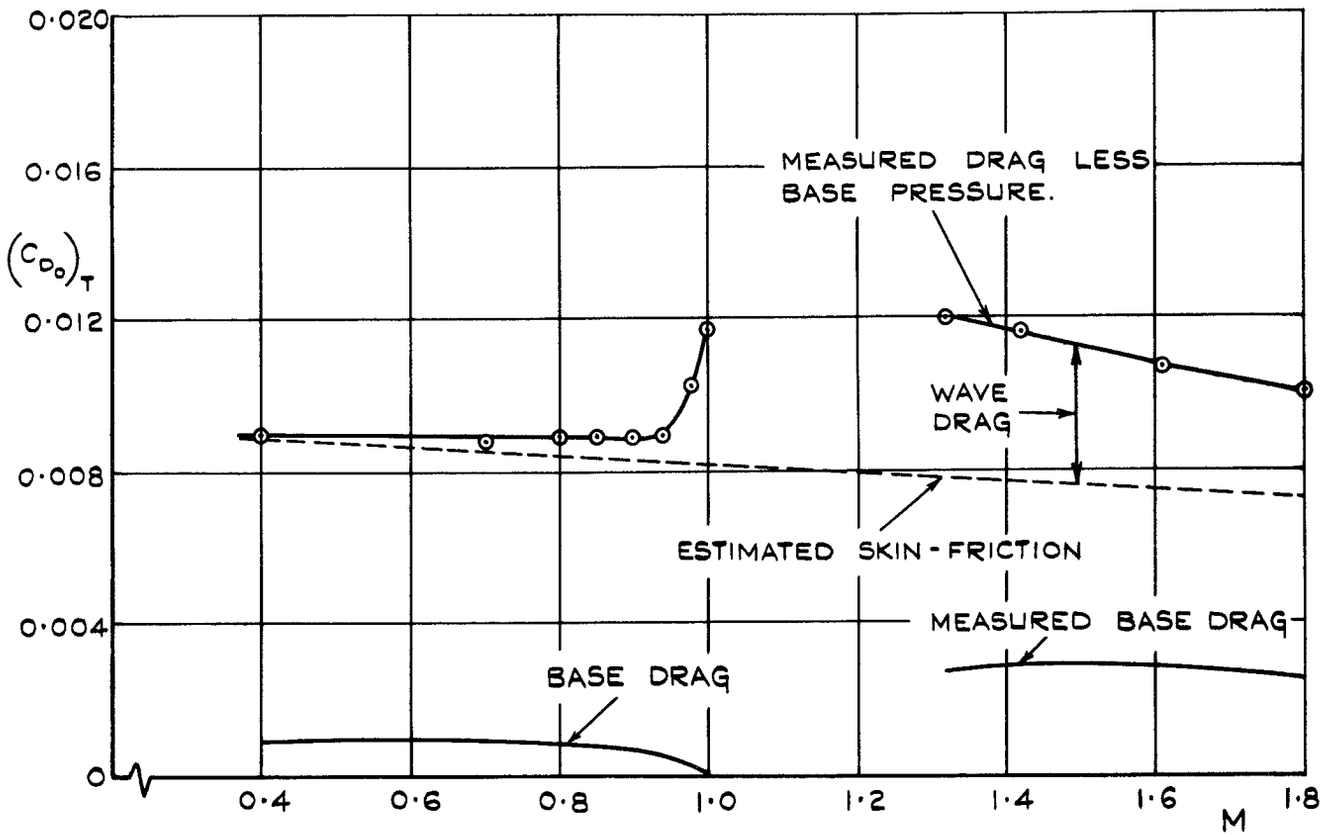

(a) MEASURED DRAG

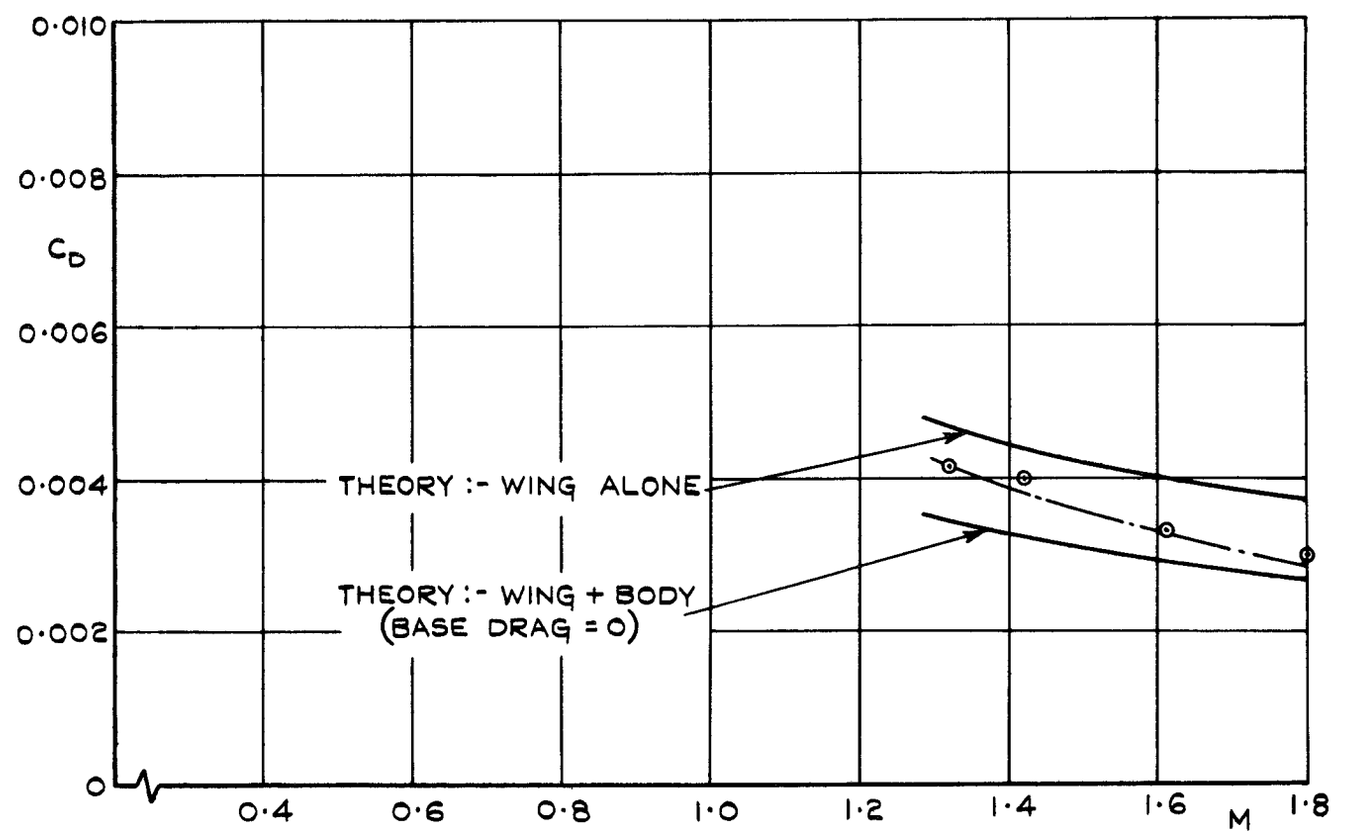

(b) WAVE DRAG

FIG. 15. VARIATION OF ZERO LIFT DRAG WITH MACH NUMBER.

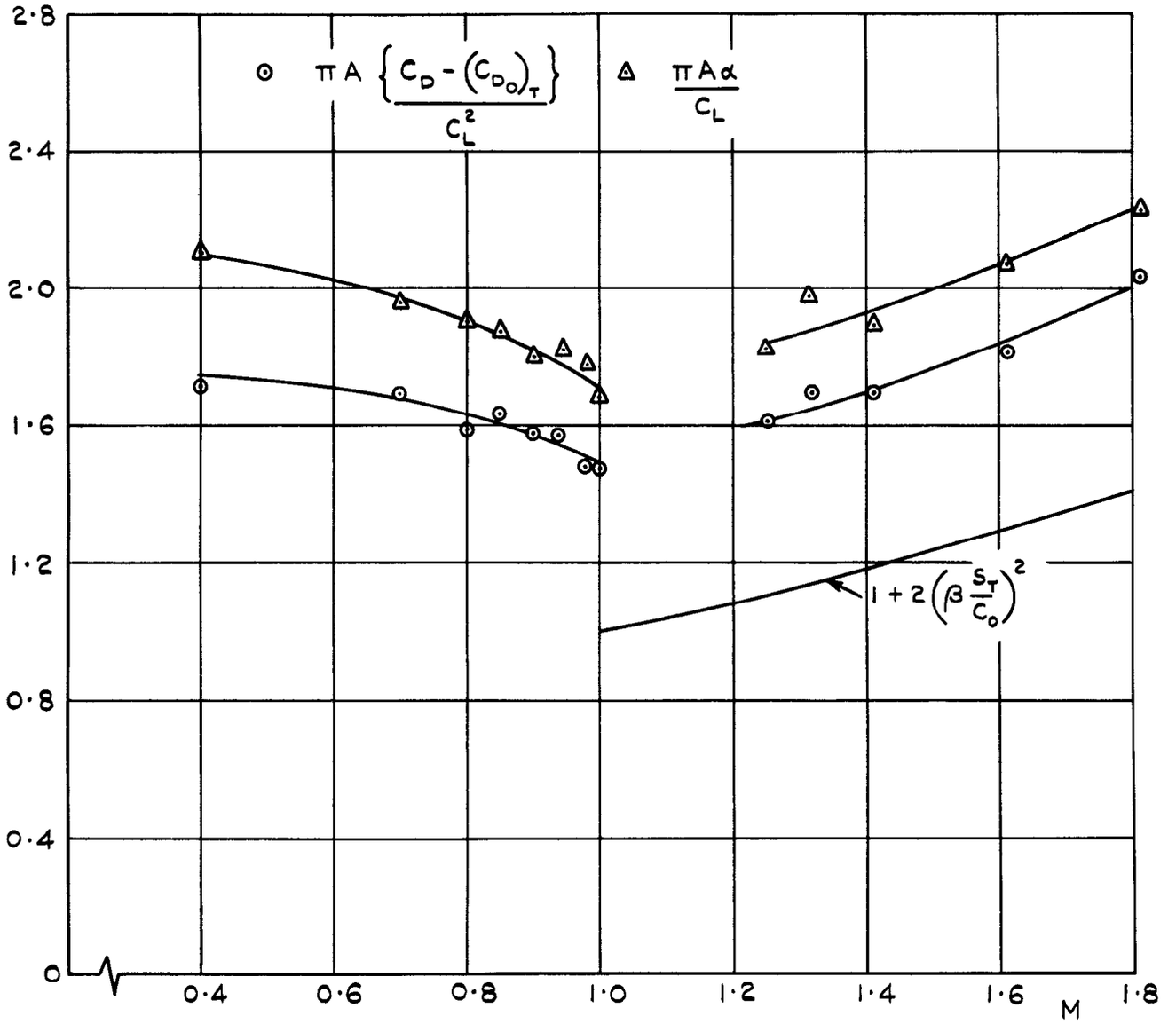

FIG. 16. VARIATION OF INDUCED DRAG FACTOR ($C_L = 0 \cdot 1$) WITH MACH NUMBER.

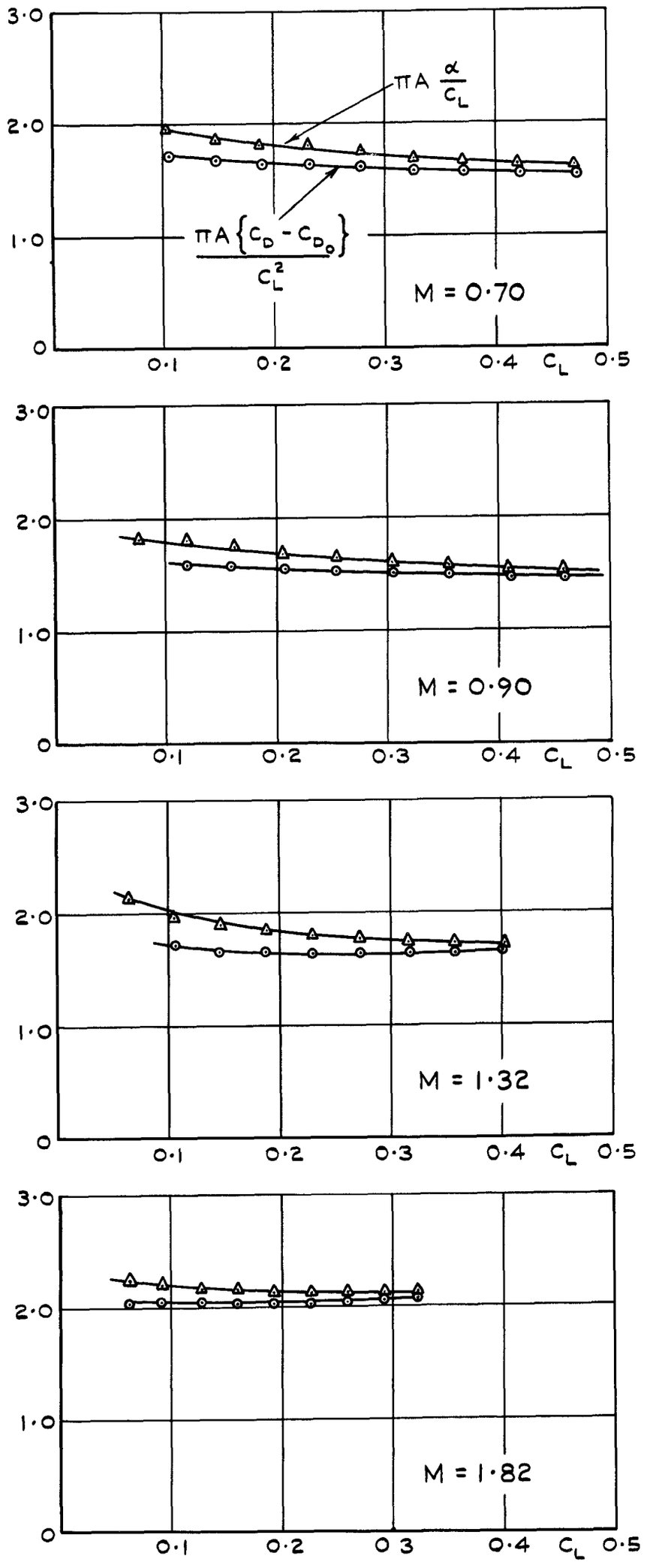

FIG. 17. VARIATION OF INDUCED DRAG FACTOR WITH C_L.

533.693.3:
533.6.011.34/5:
533.6.013.412

A.R.C. C.P. No.585

AN EXPERIMENTAL INVESTIGATION OF THE CHARACTERISTICS OF AN OGEE WING FROM M = 0.4 TO M = 1.8. Squire, L.C. and Capps, D.S. August, 1959.

Wind tunnel tests have been made in the 3 ft tunnel at R.A.E. Bedford to investigate the flow development and longitudinal static stability of a slender ogee wing (aspect ratio 1.2) from M = 0.4 to M = 1.82. Throughout the Mach number range the flow separates from the leading edge at some positive incidence and a pair of vortices lie above the wing. This leading edge separation occurs at very low incidence at subsonic speeds but at supersonic speeds occurs at progressively higher incidences as the Mach number increases. The additional lift associated with the vortices is approximately independent of Mach number at subsonic

(Over)

533.693.3:
533.6.011.34/5:
533.6.013.412

A.R.C. C.P. No.585

AN EXPERIMENTAL INVESTIGATION OF THE CHARACTERISTICS OF AN OGEE WING FROM M = 0.4 TO M = 1.8. Squire, L.C. and Capps, D.S. August, 1959.

Wind tunnel tests have been made in the 3 ft tunnel at R.A.E. Bedford to investigate the flow development and longitudinal static stability of a slender ogee wing (aspect ratio 1.2) from M = 0.4 to M = 1.82. Throughout the Mach number range the flow separates from the leading edge at some positive incidence and a pair of vortices lie above the wing. This leading edge separation occurs at very low incidence at subsonic speeds but at supersonic speeds occurs at progressively higher incidences as the Mach number increases. The additional lift associated with the vortices is approximately independent of Mach number at subsonic

(Over)

533.693.3:
533.6.011.34/5:
533.6.013.412

A.R.C. C.P. No. 585

AN EXPERIMENTAL INVESTIGATION OF THE CHARACTERISTICS OF AN OGEE WING FROM M = 0.4 TO M = 1.8. Squire, L.C. and Capps, D.S. August, 1959.

Wind tunnel tests have been made in the 3 ft tunnel at R.A.E. Bedford to investigate the flow development and longitudinal static stability of a slender ogee wing (aspect ratio 1.2) from M = 0.4 to M = 1.82. Throughout the Mach number range the flow separates from the leading edge at some positive incidence and a pair of vortices lie above the wing. This leading edge separation occurs at very low incidence at subsonic speeds but at supersonic speeds occurs at progressively higher incidences as the Mach number increases. The additional lift associated with the vortices is approximately independent of Mach number at subsonic

(Over)

speeds but at supersonic speeds the additional lift decreases with increase in Mach number. The overall rearward shift in aerodynamic centre position and centre of pressure position between subsonic and supersonic speeds is 6% of the root chord.

speeds but at supersonic speeds the additional lift decreases with increase in Mach number. The overall rearward shift in aerodynamic centre position and centre of pressure position between subsonic and supersonic speeds is 6% of the root chord.

speeds but at supersonic speeds the additional lift decreases with increase in Mach number. The overall rearward shift in aerodynamic centre position and centre of pressure position between subsonic and supersonic speeds is 6% of the root chord.

Published by
HER MAJESTY'S STATIONERY OFFICE

To be purchased from
York House, Kingsway, London w.c.2
423 Oxford Street, London w.1
13A Castle Street, Edinburgh 2
109 St. Mary Street, Cardiff
39 King Street, Manchester 2
50 Fairfax Street, Bristol 1
2 Edmund Street, Birmingham 3
80 Chichester Street, Belfast 1
or through any bookseller

Printed in England

S.O. CODE No. 23-9012-85